IEEE Access
Multidisciplinary | Rapid Review | Open Access Journal

Received 22 May 2024, accepted 4 June 2024, date of publication 6 June 2024, date of current version 24 July 2024.

Digital Object Identifier 10.1109/ACCESS.2024.3410954

RESEARCH ARTICLE

Interference Mitigation Based on Joint Optimization of NTBS 3D Positions and RIS Reflection in Downlink NOMA HetNets

OSAMAH THAMER HASSAN ALZUBAIDI[1], MHD NOUR HINDIA[1], (Member, IEEE), KAHARUDIN DIMYATI[1], (Member, IEEE), KAMARUL ARIFFIN NOORDIN[1], (Senior Member, IEEE), AND FAIZAN QAMAR[2], (Member, IEEE)

[1]Centre of Advanced Communication, Research and Innovation (ACRI), Department of Electrical Engineering, Faculty of Engineering, University of Malaya (UM), Kuala Lumpur 50603, Malaysia
[2]Centre for Cyber Security, Faculty of Information Science and Technology, Universiti Kebangsaan Malaysia (UKM), Bangi, Selangor 43600, Malaysia

Corresponding authors: Kaharudin Dimyati (kaharudin@um.edu.my) and Kamarul Ariffin Noordin (kamarul@um.edu.my)

This work was supported by the Fundamental Research Grant Scheme (FRGS), the Ministry of Higher Education (MoHE), Malaysia, under Grant FRGS/1/2020/TK0/UM/01/2.

ABSTRACT The next generation of wireless networks is poised to deliver dependable, extensive, and extremely low-latency mobile broadband communications across various industries. In this regard, reconfigurable intelligent surface (RIS)-aided non-terrestrial base station (NTBS) is crucial for developing three-dimensional (3D) networks that aim to integrate the terrestrial and non-terrestrial infrastructures. The integration of RISs with NTBSs has resulted in additional capabilities to attain faster and more flexible mobile coverage. In this paper, we employ a novel RIS-aided NTBSs with non-orthogonal multiple access in downlink heterogeneous networks (HetNets), in which the RIS is utilized to improve the transmission of signals from multiple NTBSs to ground users (GUs). We aim to maximize the system sum rate (SSR) and energy efficiency (EE) by mitigating inter-cluster and intra-cluster interference. The formulated optimization problem is non-convex due to the joint optimization of NTBS 3D positions, RIS reflection angles, RIS reflection coefficients, and successive interference cancellation among GUs. To address this problem, a modified gray wolf optimization -based meta-heuristic algorithm is proposed. In particular, the original optimization problem is divided into three sub-problems (i.e., RIS reflection angles, RIS reflection coefficients, and NTBS 3D position), which are then addressed alternately using the proposed optimization technique. The novelty of our proposed work is presented by reformulating the distance equations to minimize the distance between the wolves and their prey and enhance the search process's precision. The simulation results stated that the suggested algorithm outperforms the traditional schemes in terms of both SSR and EE. Furthermore, the results show that incorporating RIS into multi-NTBS HetNets effectively boosts overall performance by improving the channel quality between NTBSs and their respective GUs while reducing inter-NTBS interference.

INDEX TERMS B5G, MGWO, HetNets, NOMA, NTBS, RIS, SIC.

I. INTRODUCTION

The progress and affordability improvements in manufacturing technologies have led to a growing fascination with non-terrestrial base stations (NTBSs), such as unmanned

The associate editor coordinating the review of this manuscript and approving it for publication was Adao Silva.

aerial vehicles (UAVs), commonly known as drones, for their potential applications in diverse civil applications like traffic surveillance, cargo delivery, and search and rescue missions [1], [2], [3]. Among various possibilities, communication utilizing NTBSs stands out as particularly appealing. These NTBSs can function as aerial base stations, equipped with communication tools to offer wireless communication services in numerous real-world scenarios. This includes scenarios like diverting traffic to temporary hotspots or restoring communication networks following natural disasters. Unlike conventional terrestrial communications, line-of-sight (LoS) links dominate the air-to-ground (A2G) channel [4]. This leads to reliable transmission with higher data rates. Moreover, the NTBSs' mobility can be managed and used to enhance communication performance. For example, The NTBS can approach the target ground user to acquire enhanced channel characteristics.

Despite the benefits above, mitigating interference arising from the predominant LoS nature of the A2G channel, particularly in scenarios involving multiple NTBSs, is regarded as a major challenge in facilitating NTBS-enabled communication [5]. The relationship between inter-cell interference (ICI) and NTBS is critical, as these stations must carefully manage interference to ensure reliable communication across overlapping coverage areas [6], [7]. One potential approach to address this issue involves utilizing reconfigurable intelligent surfaces (RISs) proposed recently [8], [9]. A RIS is a slender artificial surface comprising numerous passive reflecting components that are economical to produce. These components are adjusted by changing their phase shifts and amplitudes, thereby modifying how incoming signals propagate. The optimization of RIS reflecting coefficients involves a combination of reflected and non-reflected signals in a manner that either amplifies the desired signal strength or eliminates interference by constructive and destructive interference, respectively [10]. Additionally, it is easy to incorporate RISs into current wireless networks due to their ability to be placed on a variety of structures, like roadside billboards, building facades, and indoor walls, providing flexibility in their deployment. This feature of RISs allows them to be conveniently integrated into different wireless networks [11].

In NTBS-based communication, NTBSs typically must provide services to a massive number of ground users (GUs) with specific communication demands. This holds particularly true for the future Beyond Fifth Generation (B5G) networks. Advanced multiple-access techniques are essential for tackling these challenges. In particular, non-orthogonal multiple access (NOMA), which maximizes spectrum efficiency (SE) and supports massive connections, is considered a potential solution for integrating NTBS into the B5G networks. [12]. NOMA enables several users to share resources at the same time and frequency. Using successive interference cancellation (SIC) methods, NOMA can distinguish among users according to their power levels. Using NOMA in NTBS communications improved by RIS is an appealing approach. It is seen as mutually beneficial because of the following factors: First, NOMA offers better elastic and effective resource allocation (RA) for NTBS communication that RIS enhances compared to the traditional orthogonal multiple access (OMA). Consequently, SE can be improved, and various users' communication needs can be covered [13]. Second, the sequencing of SIC decoding order among users in traditional NOMA transmissions is commonly calculated based on ''dumb'' channel characteristics [14], [15]. It's crucial to know that both NTBSs and RISs are channel-changing technologies. Leveraging the mobility of NTBSs and/or adjusting the reflection coefficients of RISs can enhance or degrade user channel conditions, enabling the intelligent implementation of NOMA [16].

A. RELATED WORKS

The latest research carried out on cluster interference [17], [18], [19], inter-user interference [20], [21], [22], [23], [24], ICI [25], [26], [27], and self-interference [28], [29], [30], [31], [32] schemes in RISs are presented in this subsection.

1) CLUSTER INTERFERENCE SCHEMES

In [17], the RIS-enhanced multi-UAV NOMA networks are investigated. To maximize the total data rate of the networks under consideration, the joint optimization for the UAV transmission power and three-dimensional (3D) placement, the RIS reflection coefficients, and the NOMA decoding orders among users are considered. A block coordinate descent (BCD)-based technique is evolved to identify a suboptimal solution iteratively to cope with the ensuing mixed-integer non-convex optimization problem. The simulation results proved that optimizing UAV trajectory, RIS deployment, and utilizing NOMA can substantially enhance the attained total data rate.

In [18], RIS is implemented in the NOMA network, aided by UAVs. In this network, the RIS enhances the transmission of signals from various UAVs to GUs. Since the formulated optimization problem simultaneously optimizes the UAV position, power transmission, active beamforming vectors (ABVs), reflection coefficients of RIS, and decoding order among users, it is non-convex and consequently quite challenging to solve optimally. To address this issue, the resultant optimization problem is divided into four distinct subproblems and resolved through an iterative process. First, the UAV placement sub-solution, which can be achieved via successive convex approximation (SCA) and maximum ratio transmission, is considered. The transmission power is optimized through conventional convex optimization techniques. Afterward, the reflection coefficients of RIS can be expressed in closed form by utilizing the Gaussian randomization procedure. Finally, a dynamic-decoding order technique that optimizes the NOMA decoding order is proposed to ensure user fairness. The numerical results stated that the suggested joint RA and deployment of the UAV algorithm dramatically

minimize the total power consumption compared to the conventional approaches.

In [19], the RIS is employed to improve energy efficiency (EE) and the possibilities of task-offloading in a mobile edge computing scenario that makes use of UAVs. The total sum rate of internet of things (IoT) devices is maximized by the joint optimization of time allocation, power transmission, IoT devices' central processing unit frequency, the phase shift in the energy transfer and task offloading stages, and the trajectory of UAVs. An alternative search method (ASM) is suggested to deal with the non-linear, non-convex optimization problem. The numerical results showed that the suggested ASM algorithm has superior computational performance compared to the benchmark designs.

2) INTER-USER INTERFERENCE SCHEMES

In [20], an intelligent reflecting surface (IRS)-assisted UAV reliability with limited energy of the UAV in complicated urban environments is investigated. The joint optimization of the trajectory of UAVs, the power allocation (PA) of UAVs, and the scheduling of IRS, the phase shift matrix of IRS, is presented to maximize the transmission link's reliability, taking into consideration the constraints of the energy of the UAV and the error rate of the channel. A chaotic adaptative hybrid whale optimization algorithm (CAHWOA) is designed to tackle the non-linear, non-convex original problem. The simulation results stated that the joint optimization algorithm can significantly enhance the transmission link reliability of the proposed system.

In [21], a novel framework of aerial IRS (AIRS) enhancing the NOMA system is proposed. The joint optimization of the UAV position, PA among users, and a passive beamforming of AIRS maximizes the total sum rate of the proposed system. Because of the non-convex nature of the optimization problem, it is divided into three sub-problems and alternatingly addressed using the SCA. Furthermore, the reflection matrix of the IRS is addressed through the implementation of semi-definite programming (SDP), and comparisons are conducted utilizing particle swarm optimization (PSO). The simulation results indicated that the performance of the suggested system could attain a higher data rate than that of the conventional system.

In [22], the simultaneous operation of the IRS-assisted uplink (UL) sparse code multiple access (SCMA) wireless cellular network along with device-to-device (D2D) users is considered. The average data rate of the cellular network is maximized by the joint design of IRS phase shifts, resource block association for D2D users, and transmission power for D2D users as well as cellular users. A BCD technique-based, effective iterative approach is proposed to address the non-convex original problem. The numerical results confirmed that the suggested approach is suitable and effective for addressing the optimization problem.

In [23], a framework for optimizing energy consumption in a multi-cluster simultaneous transmission and reflection (STAR) RIS-based time division multiple access (TDMA)-aided hybrid NOMA system is proposed. The EE of the proposed scenario is maximized by jointly optimizing ABVs at the transmitter, phase shifts, energy conservation, SIC-decoding order constraints, time allocation, and the transmitter and reflector coefficients under quality of service (QoS). Moreover, an alternating optimization (AO) scheme is proposed to address the non-convex problem. The numerical results showed that the proposed technique is effective in terms of EE and achieves convergence in a minimum number of iterations.

In [24], a model for communication channels involving UAV-assisted IRSs in orthogonal frequency division multiple access (OFDMA) heterogeneous networks (HetNets) has been derived. Specifically, a swarm of drones equipped with IRSs has been considered. Additionally, the IRSs are split into patches of various sizes that can be specified for several GUs. According to these presumptions, a lower-band gain expression is acquired by 1) managing the phase shifts that can be controlled in a way that lowers the degrees of freedom; 2) using a mathematical approximation to represent the complicated Gaussian product used in channel modeling; and 3) enforcing a set outage probability to deal with the channel's built-in randomness. The numerical results demonstrate that including UAVs equipped with IRS improves the quality of the GUs' channels.

3) INTER-CELL INTERFERENCE SCHEMES

In [25], a UAV with simultaneous transmission and reflection RIS (STAR RIS-UAV) scheme is investigated for enhancing wireless communication systems in multi-user networks. The total rate of the proposed system is maximized by optimizing the TRC matrices in addition to the corresponding beamforming vectors. The numerical results stated that the suggested system could substantially enhance the average system rate compared to the no-STAR-IRS and the traditional IRS schemes.

In [26], a UAV communication system that combines NOMA with simultaneous wireless information and power transfer (SWIPT) is considered to enhance the practicality of UAV-RIS networks. This original complicated non-convex problem is decomposed into three steps because of the extreme coupling among several parameters in the original problem. The first step initially divides the problem into two stages: NOMA sub-channel allocation and SIC decoding order. The objective is to determine the optimal solution for each stage independently. In the second step, a Lagrangian duality-base beamforming design is employed, taking into account the maximum power transmission of the UAV, the energy harvesting threshold of the user, the constraints of cross-layer interference, and the QoS demands of the users. In the third step, the joint optimization of the power-splitting factors and the RIS reflection phases using the penalty-semi-definite relaxation (SDR) technique is innovated to attain a near-optimal solution. The numerical results stated that implementing RISs significantly affects the EE of the proposed system.

In [27], a framework for A2G UL NOMA that employs IRSs is investigated. Flight safety is crucial when using UAVs in urban airspace. The joint optimization of the trajectory of UAVs, IRS reflection angles, and UAV transmission power are considered. The objective is to maximize the total rate of the network while ensuring the flying safety of the UAV and satisfying the minimum sum-rate requirements for both the GU and UAV. To address this optimization problem, a sample-efficient deep reinforcement learning algorithm is suggested to enhance the placement of the UAV, the configuration of the IRS, and power control simultaneously. Furthermore, a distributionally robust deep reinforcement learning algorithm is introduced to address the factors that influence the environment to ensure the performance guarantee under the worst-case scenario. The simulation results stated that the proposed algorithm outperforms traditional algorithms concerning robustness and learning efficiency.

4) SELF-INTERFERENCE SCHEMES

In [28], incorporating hybrid active-passive RIS into the UAV platform to help in downlink (DL) transmission between the multi-antenna UAV and several users is considered. The objective is to create a fair design for two networks that support UAVs. The first network, the static UAV network, involves deploying the UAV in a fixed location to provide the service for all users simultaneously. The second network, the mobile-UAV network, involves the TDMA protocol. The joint optimization of the beamforming transmission, the trajectory of UAVs, and the coefficients of RIS maximize the minimum data rate among all users. The simulation results showed that the hybrid IRS achieves a better minimum data rate enhancement than the passive IRS under the same active elements.

In [29], the problem of deploying aerial RIS is studied to facilitate the reliable delivery of data in a remote IoT scenario. In order to reduce the average age of information of the data received by the BS over time, the joint determination of device transmission power, deployment position of RIS, phase shift of RIS, and the time of data uploading is adopted. Because of the non-convex nature of the optimization problem, a BCD is proposed to divide the optimization problem formulated into various subproblems. A near-optimum solution is attained by optimizing the variables in each sub-problem separately in an alternating iterative way. The numerical results proved that the suggested algorithm outperforms the benchmark schemes in terms of enhancing the information speed.

In [30], the NOMA-based RIS-aided UAV networks are proposed to enhance the average data rate of the proposed system when a direct link is obstructed. An AO method is suggested for the non-linear, non-convex original problem. The average data rate of the proposed system is maximized by simultaneously optimizing the RIS position, RIS phase shift, successful SIC, UAV altitude, BS's maximum transmission power, and power splitting factors. The simulation results demonstrated that the suggested system can substantially enhance the total system rate compared to conventional approaches.

In [31], a combination of an IRS installed on a full-duplex UAV and splitting-rate multiple access (SRMA) is proposed to improve SE in aerial networks. The joint optimization of SRMA parameters, the UAV's trajectory, the IRS's placement, and the IRS's phase shift matrix are considered. To address the non-convex optimization problem, the resultant optimization problem is divided into three subproblems and resolved through an iterative process. First, the PA sub-solution that can be achieved via the BCD algorithm is considered. The IRS phase shift is optimized by utilizing the Riemannian conjugate gradient (RCG) algorithm. Finally, an iterative scheme is used to get the optimum position for both the IRS and UAV. The simulation results stated that RSMA is more effective than NOMA and conventional OMA schemes.

In [32], a new secure transmitting strategy is suggested for NOMA networks with RIS assistance, prioritizing security against external and internal surveillance. First, the maximization problem of the security rate is formulated, in which the phase shift matrix of RIS and the PA of NOMA are optimized. Second, to address the non-convex original problem, it is decoupled into two distinct security problems: internal and external. Then, a heuristic-simulated annealing (SA) algorithm is suggested to address decoupled non-convex problems. This algorithm uses the Lagrange multiplier method, the SDR approach, and the singular value decomposition approach to figure out the PA and phase shift.

B. MOTIVATION AND CONTRIBUTION

There is still a big research gap in using RIS for NTBS-based communication with multiple users and NTBS. Previous studies have laid a strong foundation for using NTBS-qualified and RIS-promoted communication. The above studies look into the RIS reflection angles and coefficients as well as the joint NTBS trajectory optimization problems. However, none of these studies focus on the possible performance benefits of optimum-position NTBS networks supported by RIS with DL NOMA transmission.

The main challenges of this work are identified in the following points:

- The performance of NTBS-based communication is sharply affected by several parameters such as the NTBS's altitude and the GUs' position. The deployment of NTBSs must be carefully planned to ensure optimal performance. However, when multiple NTBSs are deployed simultaneously, they can cause inter-NTBS interference [33].
- When determining the optimum altitude for the deployment of NTBSs, the probability of having a LoS link must be considered. Deploying NTBSs at lower altitudes can lead to lower coverage and lower probabilities of having LoS links due to the shadow effect. On the

contrary, NTBSs deployed at higher altitudes can suffer from poor coverage performance due to higher path losses resulting from the larger distance between the transmitter and receiver [34].

- In a multi-NTBS environment, each GU's communication rate is influenced by both the level of interference and the power strength of the desired signal. Optimizing the NTBS 3D positions requires striking a balance between the desired signal strengths conveyed to desired GUs and inter-UAV interference imposed on undesired GUs, which is a significant challenge [35].
- In contrast to the single-GU environment [36], the configuration of optimal RIS for a multi-GU environment does not simply involve aligning the phases of reflected and non-reflected signals. The RIS reflection coefficients must be shared by multiple GUs simultaneously, making their design significantly more challenging [37].
- Using NOMA adds a new way to design decoding orders based on channel conditions [38]. This leads to strong connections between NTBS 3D positions, RIS reflection angles and coefficients, and NOMA decoding orders among GUs. Therefore, it is essential to develop efficient optimization algorithms to properly benefit from NTBS supported by RIS and NOMA and effectively adjust to the quickly evolving environments of beyond-5G wireless networks.

Considering the background and observations described earlier, the main contributions of this paper can be summarized as follows:

- A novel transmission structure is proposed for several NTBS wireless communication networks, where NOMA is used at each NTBS to serve GUs. RIS is used to boost NTBS transmission to the desired GUs and reduce the impact of interference from other, non-targeted GUs. The SSR and EE maximization problems are formulated for the joint optimization of NTBS 3D positions, the RIS's reflection coefficients and reflection angles, and the NOMA-SIC at each user cluster. Moreover, a theoretical analysis is provided, and the signal-to-interference-plus-noise ratio (SINR) and maximum achievable data rate are calculated.
- A modified gray wolf optimization (MGWO)-based meta-heuristic algorithm is proposed. As the distance between each wolf and prey should be as small as possible to obtain the most accurate results, the novelty of our proposed work is presented by reformulating the distance equations to minimize the distance between the wolves and their prey and enhance the search process's precision. Based on the reformulated equations, the ability of the MGWO increased accordingly to retain information on the search space through the iteration process without configuring supplementary control parameters. The original problem is divided into three sub-problems and then tackled iteratively. The three sub-problems, namely, RIS reflection angles, RIS reflection coefficients, and NTBS 3D positions with NOMA-SIC are successfully resolved by employing the MGWO technique.
- Compared with other benchmark techniques, the proposed RIS-enhanced NTBS NOMA scheme has substantially enhanced coverage capacity, sum rate, and EE performance. Moreover, the results indicate that the inclusion of the RIS has a dual effect: it improves the channel quality between NTBSs and served GUs, while simultaneously reducing the impact of interference originating from unserved GUs. Furthermore, the advantages of NOMA over other multiple access techniques are significantly increased by optimizing the NTBSs 3D positions, as it increases the channel differences among GUs and facilitates flexible SIC design. This leads to enhanced performance gains with NOMA in the proposed system.
- The simulation results demonstrate that in terms of SSR and EE, the proposed algorithm can outperform other traditional algorithms such as BCD, Annealing, Greedy, GWO OMA, NOMA with RIS (random reflection coefficient), and NOMA without RIS. In this paper, the NOMA with RIS (random reflection coefficient) will be referred to as (NOMA+RIS), and NOMA without RIS will be referred to as (NOMA-RIS). The results also show that using the RIS with random reflection angles has the same effect on performance as without the RIS. This indicates the importance of optimizing the reflection angles and coefficients of the RIS in RIS-based communication networks.
- To the best of the author's knowledge, this is the first time that the NTBS 3D positions, RIS reflection angles, RIS reflection coefficients, and SIC among GUs have been addressed and solved using a modified evolutionary algorithm.

C. PAPER ORGANIZATION AND NOTATIONS

The sections in this paper are organized as follows: In section II, the system model for RIS-enhanced NTBSs with NOMA HetNets is presented. The formulation problem of the total sum rate maximization is presented in section III. Section IV of the paper presents the development of an optimization method designed to find a solution for the optimization problem that has been described. The simulation results are given in section V. Finally, the conclusion of this article is described in section VI.

Notation: Bold-face upper case, bold-face lower case, and lower-case characters are used to represent matrices, vectors, and scalars, respectively. The space of NX1complex-valued vectors is denoted by $\mathbb{C}^{N\times 1}$. $\mathfrak{b}^T$ and $\mathfrak{b}^H$ represent the transpose and conjugate transpose of vector $\mathfrak{b}$, respectively. The Euclidean norm, diagonal matrix, and n^{th} element of vector $\mathfrak{b}$ are represented by the notations $\|\mathfrak{b}\|$, diag $(\mathfrak{b})$, and $[\mathfrak{b}]_n$, respectively. The notation 1_{nxm} is referred to as an ''all-one'' matrix of size nxm. The notation $\mathbb{H}^N$ represents the set of all N-dimensional complex Hermitian matrices.

II. PROPOSED SYSTEM MODEL

The explored RIS-enhanced NTBSs, with NOMA in DL HetNets, are depicted in Fig. 1, where U NTBSs are utilized to support U different user clusters with the help of RIS consisting of $\mathcal{N}$ reflective elements. A feasible use of the described setup involves utilizing NTBSs to deliver communication services to transient hotspots in suburban or rural areas. It is assumed that both NTBSs and GUs have a single antenna. The set $\mathrm{U} = \{1, \cdots, \mathrm{U}\}$ is used to represent both NTBSs and their corresponding served user clusters. The set $\mathrm{M}_u = \{1, \cdots, \mathrm{M}_u\}$, $\forall\ \mathrm{u} \in \mathrm{U}$, is used to index the GUs in each cluster, where M_u stands for the number of GUs in the U^{th} cluster. A 3D Cartesian coordinate system is taken into consideration without losing its generality, and the index (u, i) is used to represent the i^{th} user in the u^{th} cluster. The positions of the $(\mathrm{u}, i)^{\text{th}}$ user, RIS, and NTBSs are fixed at $\mathfrak{W}_i^u = [x_i^u, y_i^u, z_i^u]^T$, $\forall_i \in \mathrm{M}_u$, $u \in U$, $\mathfrak{q} = [x_{\mathfrak{q}}, y_{\mathfrak{q}}, z_{\mathfrak{q}}]^T$, and $\boldsymbol{\Psi}_u = [x_u, y_u, z_u]^T$, respectively. In order to maintain safe operation and prevent collisions, certain restrictions must be followed regarding the altitude at which NTBSs fly and the minimum distance that must be maintained between any two NTBSs, as follows:

$$Z_{max} \geq z_u \geq Z_{min}, \quad \forall u \in \mathrm{U} \tag{1}$$

$$\left\| \boldsymbol{\Psi}_u - \boldsymbol{\Psi}_j \right\| \geq \Delta_{min}, \quad \forall u \neq j \in U \tag{2}$$

The range of permissible altitudes for NTBS is denoted by $[\mathrm{Z_{max}}, \mathrm{Z_{min}}]$ while the minimum distance between any two NTBSs to prevent collisions is represented as "Δ_{min}".

In practical applications, it is common for RIS to be equipped with an advanced controller, such as a field-programmable gate array (FPGA), which is responsible for setting and adjusting reflection coefficients, as well as facilitating communication and information exchange between the RIS and NTBSs [39]. The NTBS-RIS-user connection has considerable path loss, requiring a substantial number of reflecting components to provide a reflection link with path loss equivalent to the unobstructed direct NTBS-user link. However, this results in an unreasonably large overhead and a high level of complexity regarding channel acquisition and the design or reconfiguration of the reflection coefficient. To solve this problem, the RIS is partitioned into smaller sub-surfaces with a higher channel correlation. Assume that each sub-surface is composed of a different reflecting element.

It is assumed that each sub-surface's reflecting element has the same or a different reflection coefficient. The reflection matrix of the RIS is represented as $\mathcal{b} = \phi.\mathrm{dia\,g}\left(\boldsymbol{\theta} * \mathbf{1}_{\mathrm{N}\times 1}\right) \in \mathbb{C}^{\mathrm{N}\times\mathrm{N}}$, where $\boldsymbol{\theta} = \left[e^{j\boldsymbol{\theta}_1}, e^{j\boldsymbol{\theta}_2}, \ldots, e^{j^{\boldsymbol{\theta}}\mathcal{N}}\right]^T$, $\boldsymbol{\theta}_n \in (0, 2\pi)$, and $\boldsymbol{\phi}_n \in (0, 1)\ \forall n \in \mathcal{N} = 1, \ldots, \mathcal{N}$ represents the reflection angle and reflection coefficient associated with the n^{th} sub-surface of the RIS, respectively.

In the following two sub-sections, we will provide a detailed theoretical analysis of our proposed system. The first sub-section (the model of channel) provides a detailed theoretical framework of the channel models used in our proposed system, including the mathematical representations and assumptions necessary for the subsequent analysis of channel behaviors. while the second sub-section (NOMA transmission) elaborates on the theoretical underpinnings of NOMA techniques, discussing how they are applied within our proposed system model.

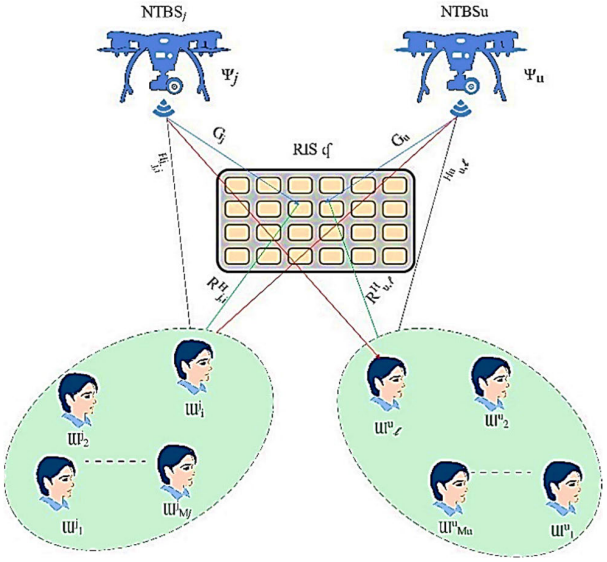

FIGURE 1. RIS-enhanced several-NTBS NOMA HetNets.

A. THE MODEL OF CHANNEL

Let $\mathcal{H}_{u,i}^j \in \mathbb{C}^{1\times 1}$ refers to the communication channel between the $\boldsymbol{j^{th}}$ NTBS and the $(\boldsymbol{u}, \boldsymbol{i})^{\boldsymbol{th}}$ GU, $\boldsymbol{r_{u,i}} \in \mathbb{C}^{\mathrm{N}\times 1}$ refers to the communication channel between the RIS and the $(\boldsymbol{u}, \boldsymbol{i})^{\boldsymbol{th}}$ GU, and $\mathfrak{g}_u \in \mathbb{C}^{\mathrm{N}\times 1}$ refers to the communication channel between the $\boldsymbol{u^{th}}$ NTBS and the RIS, since NTBSs often fly at elevated altitudes, are strategically deployed to prevent the blockage of a signal. The channels $\mathcal{H}_{\boldsymbol{u,i}}^{\boldsymbol{j}}$ and $\boldsymbol{r_{u,i}}$ models are supposed to be the "Rician channel model", which is mathematically expressed as:

$$\mathcal{H}_{u,i}^j = \sqrt{\frac{\mathfrak{d}}{\left|\boldsymbol{\psi}_j - \mathfrak{W}_i^u\right|^{\alpha_1}}} \left(\varrho_1 \sqrt{\beta_1} \bar{\mathcal{H}}_{u,i}^j + \varrho_1 \tilde{\mathcal{H}}_{u,i}^j\right) \tag{3}$$

$$\boldsymbol{r}_{k,i} = \sqrt{\frac{\mathfrak{d}}{\left|\mathfrak{q} - \mathfrak{W}_i^u\right|^{\alpha_2}}} \left(\varrho_2 \sqrt{\beta_2} \boldsymbol{r}_{u,i} + \varrho_2 \tilde{\boldsymbol{r}}_{u,i}\right) \tag{4}$$

where $\mathfrak{d}$ denotes the path loss that is measured at a standardized distance of one meter. The values $\alpha_1 \geq 2$ and $\alpha_2 \geq 2$ represents the path loss exponents (PLEs) for the links between the NTBS and user, and between the RIS and user, respectively. β_1 and β_2 represent the Rician factors, $\varrho_1 = \sqrt{\frac{1}{\beta_1+1}}$ and $\varrho_2 = \sqrt{\frac{1}{\beta_2+1}}$, $\bar{\mathcal{H}}_{u,i}^j = 1$ and $\bar{\boldsymbol{r}}_{u,i}$ represent the deterministic LoS components, and $\tilde{\mathcal{H}}_{u,i}^j$ *and* $\tilde{\boldsymbol{r}}_{u,i}$ represent the random components of non-line-of-sight (NLoS) Rayleigh distribution. More specifically, like [17], a uniform

linear array (ULA) is taken into consideration for RIS and $\bar{\boldsymbol{r}}_{u,i}$ is given by:

$$\bar{\boldsymbol{r}}_{u,i} = \left[e^{-j\frac{2\pi}{\lambda}\gamma\partial cos\,\psi_{u,i}}\right]^T \tag{5}$$

λ represents the carrier signal wavelength, γ represents the spacing between elements in the given context, $\partial = [0, 1, 2, \ldots\ldots, (N\text{-}1)]$, and $cos\,\psi_{u,i} = \frac{x_i^u - x_{\mathfrak{q}}}{\|w_i^u - \mathfrak{q}\|}$ refers to the cosine of the $(u,i)^{th}$ user's Angle of Departure from the RIS.

In addition, $\mathfrak{g}_u$ is supposed to represent the LoS channel for the NTBS-RIS channel and can be stated as

$$\mathfrak{g}_u = \sqrt{\frac{\mathfrak{d}}{\|\Psi_u - \mathfrak{q}\|^2}}\,\bar{\mathfrak{g}}_u = \sqrt{\frac{\mathfrak{d}}{\|\Psi_u - \mathfrak{q}\|^2}}\left[e^{-j\frac{2\pi}{\lambda}\gamma\partial cos\,\sigma_u}\right]^T \tag{6}$$

where $cos\,\sigma_u = \frac{x_{\mathfrak{q}} - x_u}{\|\mathfrak{q} - \Psi_u\|}$ is the cosine of the angle of arrival from the U^{th} NTBS to the RIS.

According to the channel models mentioned above, the efficient power gain of the communication channel between the i^{th} NTBS and the $(u,i)^{th}$ user with the assistance of the RIS can be obtained as follows:

$$\mathcal{C}_{u,i}^{j} = \left|\mathcal{D}_j\right|^2, \quad \forall u, j \in U, i \in \mathcal{M}_u \tag{7}$$

where: $\mathcal{D}_j = \left|\mathcal{H}_{u,i}^{j} + \boldsymbol{r}_{u,i}{}^H \mathcal{b}\mathfrak{g}_j\right|^2$

B. NOMA TRANSMISSION

In this paper, it is supposed that NTBSs are intended to function within the same frequency range and use NOMA to establish connections with GUs. To enable the transmission of NOMA, the signal transmitted from the $\boldsymbol{u^{th}}$ NTBS to the $\boldsymbol{u^{th}}$ cluster is formulated using SIC as given by:

$$\overline{\mathcal{S}_k} = \sum_{i=1}^{M_u} \sqrt{\mathcal{P}_{u,i}}\mathcal{S}_{u,i} \tag{8}$$

where the transmitted signal is represented by $\mathcal{S}_{u,i}$ and the transmitted power is represented by $\mathcal{P}_{u,i}$ for the $(u,i)^{th}$ user. We have

$$\sum_{i=1}^{M_u} \mathcal{P}_{k,i} \le P_{max,u}, \quad \forall u \in U \tag{9}$$

where $P_{max,u}$ stands for the u^{th} NTBS's maximum transmission power. Following that, the signal received by the $(u,i)^{th}$ user can be represented as:

$$\begin{aligned} y_{u,i} = {} & \underbrace{\left(\mathcal{H}_{u,i}^{j} + \mathcal{D}_u\right)\sqrt{\mathcal{P}_{u,i}}\mathcal{S}_{u,i}}_{\text{desired signal}} \\ & + \underbrace{\left(\mathcal{H}_{u,i}^{j} + \mathcal{D}_u\right)\sum_{t=1,t\neq i}\sqrt{\mathcal{P}_{u,t}}\mathcal{S}_{u,t}}_{\text{intra-cluster interference}} \\ & + \underbrace{\sum_{j=1,j\neq u}^{U}\left(\mathcal{H}_{u,i}^{j} + \mathcal{D}_j\right)\sum_{\ell=1}^{M_j}\sqrt{\mathcal{P}_{j,\ell}}\mathcal{S}_{j,\ell}}_{\text{inter-cluster interference}} + \mathcal{n}_{u,i} \end{aligned} \tag{10}$$

where $\mathcal{D}_j = \boldsymbol{r}_{u,i}{}^H \mathcal{b}\mathfrak{g}_u$, $\mathcal{n}_{u,i}$ stands for an additive white Gaussian noise (AWGN) with a mean of zero and a variance of σ^2.

Each user uses SIC following the NOMA protocol to eliminate intra-cluster interference. Specifically, the user with a higher channel power gain is seen to first decode the signal of the user with a lower channel power gain, followed by decoding their signal [40], [41]. To indicate the decoding orders among GUs in each cluster, a group of binary variables is introduced, $\mathfrak{o}_{t,i}^{u} \in 0, 1, \forall u \in U, \forall t, i \in \mathcal{M}_u$. Suppose that the u^{th} NTBS is providing service to a set of GUs. If the efficient channel power gain of the $(u,t)^{th}$ user is greater than that of the $(u,i)^{th}$ user,we have $\mathfrak{o}_{t,i}^{u} = 1$; otherwise, $\mathfrak{o}_{t,i}^{u} = 0$. Therefore, for all $u \in U, i \neq t \in \mathcal{M}_u$, $\left\{\mathfrak{o}_{t,i}^{u}\right\}$ must meet the following provisions:

$$\mathfrak{o}_{t,i}^{u} = \begin{cases} 1, & \text{if } \mathcal{C}_{u,t}^{u} \ge \mathcal{C}_{u,i}^{u} \\ 0, & \text{otherwise} \end{cases} \tag{11}$$

$$\mathfrak{o}_{t,i}^{u} + \mathfrak{o}_{i,t}^{u} = 1 \tag{12}$$

Additionally, the assigned power must meet the following criteria for the specified decoding orders:

$$\mathcal{P}_{u,i} \ge \mathfrak{o}_{t,i}^{u}\mathcal{P}_{t,i}, \quad \forall i \neq t \in \mathcal{M}_u, u \in U \tag{13}$$

This condition guarantees that GUs with lower channel power gains receive more PA compared to GUs with higher channel power gains [42],

$$\text{i.e.,} \mathcal{P}_{u,i} \ge \mathcal{P}_{k,t}, \text{ if } \mathfrak{o}_{t,i}^{u} = 1 \tag{14}$$

Consequently, the SINR received by the $(u,i)^{th}$ user after implementing SIC can be expressed as:

$$\mathfrak{z}_{u,i} = \frac{\mathcal{C}_{u,i}^{u}\,\mathcal{P}_{u,i}}{\mathfrak{g}_{u,i}^{\text{intra}} + \mathfrak{g}_{u,i}^{\text{inter}} + \sigma^2}, \quad \forall i \in \mathcal{M}_u, u \in U \tag{15}$$

where:

$$\mathfrak{g}_{u,i}^{\text{intra}} = \mathcal{C}_{u,i}^{u}\sum_{t=1,t\neq i}^{M_u}\mathfrak{o}_{t,i}^{u}\mathcal{P}_{u,t} \tag{16}$$

and

$$\mathfrak{g}_{u,i}^{\text{inter}} = \sum_{j=1,j\neq u}^{U}\mathcal{C}_{u,i}^{j}\sum_{\ell=1}^{M_j}\mathcal{P}_{j,\ell} \tag{17}$$

The attainable transmission rate for the $(u,i)^{th}$ user is given by:

$$\mathcal{R}_{u,i} = log_2\left(1 + \mathfrak{z}_{u,i}\right), \forall i \in \mathcal{M}_u, u \in U \tag{18}$$

III. PROBLEM FORMULATION OF THE PROPOSED SYSTEM

Our objective is to solve the optimization problem which is decomposed into three sub-problems (NTBS 3D positions Ψ, the RIS's reflection angles $\boldsymbol{\theta}$, the RIS's reflection coefficients $\boldsymbol{\phi}$) aiming to maximize the SSR and EE of all GUs in the network. The following equations represent the optimization problem for our proposed method:

Let $\wp = \{\Psi_u, \forall u \in U\}, \boldsymbol{P} = \{\mathcal{P}_{u,i}, \forall u \in U, i \in \mathcal{M}_u\}$, and $\mathfrak{Z} = \left\{\mathfrak{o}^u_{t,i}, \forall u \in U, i \neq t \in \mathcal{M}_u\right\}$,

$$\max_{\wp,\boldsymbol{\theta},\boldsymbol{\phi}} \sum_{u=1}^{U} \sum_{i=1}^{M_u} \overline{\mathcal{R}}_{u,i} \tag{19a}$$

$$s.t.\ Z_{max} \geq z_u \geq Z_{min}, \forall u \in U \tag{19b}$$

$$\left\|\boldsymbol{\Psi}_u - \boldsymbol{\Psi}_j\right\|^2 \geq \Delta^2_{min}, \forall u \neq j \in U \tag{19c}$$

$$\boldsymbol{\theta} = diag\left(\boldsymbol{\theta}_1, \ldots\ldots \boldsymbol{\theta}_{\mathcal{N}}\right),\ \boldsymbol{\theta}_1, \ldots\ldots \boldsymbol{\theta}_{\mathcal{N}} \in (0, 2\pi) \tag{19d}$$

$$\boldsymbol{\phi} = diag\left(\phi_1, \ldots\ldots \phi_{\mathcal{N}}\right),\ \phi_1, \ldots\ldots \phi_{\mathcal{N}} \in (0, 1) \tag{19e}$$

$$\mathcal{P}_{u,i} \geq 0, \forall u \in U, i \in \mathcal{M}_u \tag{19f}$$

$$\sum_{i=1}^{M_u} \mathcal{P}_{u,i} \leq P_{max,u}, \forall u \in U \tag{19g}$$

$$\mathcal{P}_{u,i} \geq \mathfrak{o}^u_{t,i}\, \mathcal{P}_{u,t}, \forall i \neq t \in \mathcal{M}_u, u \in U \tag{19h}$$

$$\mathfrak{o}^u_{t,i} = \begin{cases} 1, & \text{if } \|\Psi_u - \mathfrak{W}^u_t\| \leq \|\Psi_u - \mathfrak{W}^u_i\| \\ 0, & \text{otherwise,} \end{cases}$$

$$\forall u \in U, i \neq t \in \mathcal{M}_U \tag{19i}$$

$$\mathfrak{o}^u_{t,i} + \mathfrak{o}^u_{i,t} = 1, \forall u \in U, i \neq t \in \mathcal{M}_u \tag{19j}$$

The range of permissible NTBS flying heights, denoted by (19b), is designed to guarantee a secure distance between any two NTBSs. The restriction on the phase shift and reflection index of each sub-surface of an IRS is indicated by (19d), and (19e), respectively. The constraints on the transmission power of NTBS are represented by (19f) -(19h). Moreover, according to (19i), the stronger user is identified as the user who is paired with the closer NTBS. Furthermore, (19j) ensures that both GUs are not assigned as either stronger or weaker GUs when $\|\Psi_u - \mathfrak{W}^u_t\| = \|\Psi_u - \mathfrak{W}^u_i\|$.

Nevertheless, the problem (19) is difficult to be solved because of the following reasons:

- The interrelation among the optimization variables is significant, and the objective function does not exhibit concavity or convexity concerning the optimization variables.
- The design of the NOMA-SIC adds binary variables, causing integer constraints to be involved in (19h) – (19j).

Thus, problem (19) becomes a challenging non-convex optimization problem (NCOP), and it is hard to discover a globally optimum solution. The MGWO system uses the proposed technique to offer an effective iterative approach for discovering a high-quality suboptimal solution.

IV. OPTIMIZATION ALGORITHM

This paper uses a gray wolf optimization (GWO) algorithm that is based on nature to find the best coefficients and reflection angles for the RIS and the best 3D position for the NTBS in the DL HetNets. The hunting behavior of gray wolves inspires the GWO algorithm, which has no control parameters. Hence, no more parameters are required except for the parameters of maximum iterations or generations and population size [43], [44].

A. GRAY WOLF OPTIMIZATION

The GWO is described in the following sub-sections, according to the work in [43].

1) INSPIRATION

The algorithm classifies the wolf vectors into four distinct categories, namely alpha (α), beta (β), delta (δ), and omega (ω). In terms of their power values and associations, three top-performing vectors (α), (β) and (δ) have been selected for these categories. The unclassified solutions are placed in the (ω) category. These population categories (α), (β), and (δ) control the optimization process, which is comparable to group hunting behavior in a wolf pack. Grey wolves possess the capability to identify prey's location and encircle them. Typically, the (α) is in charge of the hunt. On occasion, the (β) and (δ) may also engage in hunting activities. However, the prey (optimal location) is unknown within an abstract search space. To mathematically model the grey wolves' hunting behavior, we assume that the best candidate solution (α), the second-best solution (β), and the third-best solution (δ) have the best knowledge about the prey's possible location. So, we keep track of the best three solutions found so far and make sure that all the other search agents (SAs), including the omegas, adjust their positions based on the location of the best three SAs.

2) MATHEMATICAL MODEL

The GWO technique utilizes mathematical models of how grey wolves organize themselves and hunt in the wild. One notable characteristic of this approach is its ability to retain information on the search space through the iteration process without configuring supplementary control parameters. The mathematical formulas used in the algorithm represent the encirclement of prey during a hunting process as follows:

$$\overrightarrow{\mathcal{V}}_{\xi} = \left|\overrightarrow{\mathcal{C}^2} \cdot \overrightarrow{\mathcal{Z}_{\xi}} - \overrightarrow{\mathcal{Y}}_{\xi}\right| \tag{20}$$

$$\overrightarrow{\mathcal{Y}}_{\xi+1} = \overrightarrow{\mathcal{Z}_{\omega}} - \overrightarrow{\mathcal{C}^1} \cdot \overrightarrow{\mathcal{V}_{\omega}} \tag{21}$$

$$\overrightarrow{\mathcal{C}^1} = 2\overrightarrow{\mathfrak{a}} \cdot \vec{r}_1 - \overrightarrow{\mathfrak{a}} \tag{22a}$$

$$\overrightarrow{\mathcal{C}^2} = 2 \cdot \vec{r}_2 \tag{22b}$$

where the vectors $\vec{r}_1$ and $\vec{r}_2$ are obtained randomly from a uniform distribution with values ranging from 0 to 1. The parameter ($\overrightarrow{\mathfrak{a}} \in [2, 0]$ is the parameter that is responsible for controlling the tradeoff between exploration and exploitation. The parameter " ($\overrightarrow{\mathfrak{a}}$" is updated linearly in each iteration based on the following equation:

$$\overrightarrow{\mathfrak{a}} = 2 - \xi . \frac{2}{\boldsymbol{\mu_i}} \tag{23}$$

where μ_i is the total number of iterations permitted for the optimization.

$$\overrightarrow{\mathcal{V}_{\alpha}} = \left| \overrightarrow{\mathcal{C}_1^2} \cdot \vec{\mathcal{Y}}_{\alpha} - \vec{\mathcal{Y}} \right| \tag{24a}$$

$$\overrightarrow{\mathcal{V}_{\beta}} = \left| \overrightarrow{\mathcal{C}_2^2} \cdot \vec{\mathcal{Y}}_{\beta} - \vec{\mathcal{Y}} \right| \tag{24b}$$

$$\overrightarrow{\mathcal{V}_{\delta}} = \left| \overrightarrow{\mathcal{C}_3^2} \cdot \vec{\mathcal{Y}}_{\delta} - \vec{\mathcal{Y}} \right| \tag{24c}$$

where $\overrightarrow{\mathcal{V}_{\alpha}}$ represents the distance between the alpha wolf and the prey, $\overrightarrow{\mathcal{V}_{\beta}}$ is the distance between beta wolf and prey, and $\overrightarrow{\mathcal{V}_{\delta}}$ the distance between delta wolf and prey. $\vec{\mathcal{Y}}_{\alpha}$ refers to the location of the alpha wolf, $\vec{\mathcal{Y}}_{\beta}$ represents the location of the beta wolf, $\vec{\mathcal{Y}}_{\delta}$ is the location of the delta wolf. $\vec{\mathcal{Y}}$ represents the location of prey. Note that the values of $\overrightarrow{\mathcal{V}_{\alpha}}$, $\overrightarrow{\mathcal{V}_{\beta}}$, $\overrightarrow{\mathcal{V}_{\delta}}$ are fractions (less than one).

$$\vec{\mathcal{Y}}_{\mathbf{1}} = \vec{\mathcal{Y}}_{\alpha} - \overrightarrow{\mathcal{C}_1^1} \cdot \left(\vec{\mathcal{V}}_{\alpha} \right) \tag{25a}$$

$$\vec{\mathcal{Y}}_{\mathbf{2}} = \vec{\mathcal{Y}}_{\beta} - \overrightarrow{\mathcal{C}_2^1} \cdot \left(\vec{\mathcal{V}}_{\beta} \right) \tag{25b}$$

$$\vec{\mathcal{Y}}_{\mathbf{3}} = \vec{\mathcal{Y}}_{\delta} - \overrightarrow{\mathcal{C}_3^1} \cdot \left(\vec{\mathcal{V}}_{\delta} \right) \tag{25c}$$

$$\vec{\mathcal{Y}}_{\boldsymbol{\xi+1}} = \vec{\mathcal{Y}}_{\mathbf{1}} + \vec{\mathcal{Y}}_{\mathbf{2}} + \vec{\mathcal{Y}}_{\mathbf{3}}/\mathbf{3} \tag{26}$$

where $\vec{\mathcal{Y}}_1$ represents the position that we are supposed to be in if we only follow the alpha, $\vec{\mathcal{Y}}_2$ is the position that we are supposed to be in if we only follow the beta, and $\vec{\mathcal{Y}}_3$ refers to the position that we are supposed to be in if we only follow the delta. $\vec{\mathcal{Y}}_{\xi+1}$ is the new location of the prey.

B. THE PROPOSED ALGORITHM

The goal of the proposed algorithm is to find the optimal values for the 3D positions and transmit power of NTBS, as well as the best RIS reflection angles, RIS reflection coefficients, and NOMA-SIC among GUs in each cluster to maximize the SSR and EE of all GUs in the network. The distance between each wolf and prey should be as small as possible to obtain the most accurate results. However, one of the main drawbacks of the default GWO is the large distance between the wolves and prey, leading to a lower total sum rate in the system, which affects the QoS negatively. Therefore, in the proposed algorithm, equation (23) is reformulated to minimize the distance between the wolves and their prey and enhance the search process's precision.

The equations (24a, 24b, and 24c) are reformulated as follows:

$$\overrightarrow{\mathcal{V}_{\alpha o}} = \left| \overrightarrow{\mathcal{C}_1^2} \cdot \vec{\mathcal{Y}}_{\alpha} - \vec{\mathcal{Y}} \right|^2 \tag{27a}$$

$$\overrightarrow{\mathcal{V}_{\beta o}} = \left| \overrightarrow{\mathcal{C}_2^2} \cdot \vec{\mathcal{Y}}_{\beta} - \vec{\mathcal{Y}} \right|^2 \tag{27b}$$

$$\overrightarrow{\mathcal{V}_{\delta o}} = \left| \overrightarrow{\mathcal{C}_3^2} \cdot \vec{\mathcal{Y}}_{\delta} - \vec{\mathcal{Y}} \right|^2 \tag{27c}$$

where $\overrightarrow{\mathcal{V}}_{\alpha o}$ is the modified distance between the alpha wolf and prey, $\overrightarrow{\mathcal{V}}_{\beta o}$ represents the modified distance between beta wolf and prey, and $\overrightarrow{\mathcal{V}}_{\delta o}$ refers to the modified distance between delta wolf and prey.

$$\vec{\mathcal{Y}}_{1o} = \vec{\mathcal{Y}}_{\alpha} - \overrightarrow{\mathcal{C}_1^1} \cdot \left(\overrightarrow{\mathcal{V}}_{\alpha o} \right) \tag{28a}$$

$$\vec{\mathcal{Y}}_{2o} = \vec{\mathcal{Y}}_{\beta} - \overrightarrow{\mathcal{C}_2^1} \cdot \left(\overrightarrow{\mathcal{V}}_{\beta o} \right) \tag{28b}$$

$$\vec{\mathcal{Y}}_{3o} = \vec{\mathcal{Y}}_{\delta} - \overrightarrow{\mathcal{C}_3^1} \cdot \left(\overrightarrow{\mathcal{V}}_{\delta o} \right) \tag{28c}$$

$$\vec{\mathcal{Y}}_{\xi o+1} = \vec{\mathcal{Y}}_{1o} + \vec{\mathcal{Y}}_{2o} + \vec{\mathcal{Y}}_{3o}/3 \tag{29}$$

where $\vec{\mathcal{Y}}_{1o}$ is the modified position that we are supposed to be if we only follow the alpha, $\vec{\mathcal{Y}}_{2o}$ refers to the modified position that we are supposed to be in if we only follow the beta, and $\vec{\mathcal{Y}}_3$ represents the modified position that we are supposed to be if we only follow the delta. $\vec{\mathcal{Y}}_{\xi o+1}$ is the modified new location of the prey.

The MGWO algorithm seeks to optimize the RIS reflection angles by adjusting the position of each wolf in the solution space, where each position corresponds to a set of RIS reflection angles.

The connection between the MGWO algorithm and RIS reflection angle optimization involves:

- Initialization: Each wolf's position represents a possible solution set of RIS reflection angles.
- Fitness Evaluation: We evaluate each position based on its ability to maximize SSR, which directly links the search dynamics of the MGWO to the formulated problem of sum rate maximization.
- Adaptation and Update: Equations (27, 28, and 29) iteratively update the wolves' positions towards optimal angles that yield the best SSR, using the social hierarchy and hunting behavior mimicked in MGWO.

We repeat the same procedure for optimizing the reflection coefficients and NTBS 3D positions.

C. OPTIMIZE THE RIS REFLECTION ANGLES AND COEFFICIENTS AS WELL AS NTBS 3D POSITIONS

In this sub-section, we optimize the SSR of the proposed system by considering the relevant constraints. We formulate the optimization objective function and utilize the MGWO approach to address the optimization problem. The MGWO is formulated by considering the NTBS 3D positions IRS reflection angles, and the IRS reflection coefficients.

The distance from the NTBS to the GUs and from the NTBS to the RIS are two key factors affecting performance in the proposed system. The total sum rate will change based on the NTBS 3D positions. As the NTBS 3D positions change, the sum rate of the proposed system will also change. This is because the variation in the NTBS 3D positions leads to a change in the distance between the NTBS and the RIS and the distance between the NTBS and GUs, which enhances the quality of the LoS channel. Therefore, after optimizing the IRS reflection angles and coefficients, the

NTBS 3D positions must also be optimized to find the best NTBS 3D positions for supporting the GUs.

The optimization of ($\boldsymbol{\theta}$, $\boldsymbol{\phi}$, and Ψ) is described as follows:

1) OPTIMIZING θ FOR GIVEN Ψ AND ϕ

For given Ψ and $\boldsymbol{\phi}$, the RIS reflection angle optimization problem can be written as

$$\max_{\boldsymbol{\theta}} \sum_{u=1}^{U} \sum_{n=1}^{\mathrm{N}} \overline{\mathcal{R}}_{sum} \tag{30a}$$

$$\text{s.t. (19d)} \tag{30b}$$

However, problem (30) is non-convex because the objective function is non-concave, and the unit-modulus constraint (19d) is non-convex. As described in algorithm 1, the process begins by assuming all initial reflection coefficients are set to one and making a random selection of RIS reflection angle elements and a random selection of other elements in a way that meets the QoS requirements. A 2D matrix is created to represent the RIS reflection angles.

2) OPTIMIZING ϕ FOR GIVEN Ψ AND θ

For given Ψ and $\boldsymbol{\theta}$, the RIS reflection coefficients optimization problem can be written as

$$\max_{\boldsymbol{\phi}} \sum_{u=1}^{U} \sum_{n=1}^{\mathrm{N}} \overline{\mathcal{R}}_{sum} \tag{31a}$$

$$\text{s.t. (19e)} \tag{31b}$$

However, problem (31) is non-convex because the objective function is non-concave, and the unit-modulus constraint (19e) is non-convex. We optimize the RIS reflection coefficients depending on the optimal RIS reflection angles and a random selection of other elements in a way that meets the QoS requirements. A 2D matrix is also created to represent the RIS reflection coefficients.

3) OPTIMIZING Ψ FOR GIVEN θ AND ϕ

For given $\boldsymbol{\theta}$ and $\boldsymbol{\phi}$, the NTBS 3D positions optimization problem can be written as

$$\max_{\boldsymbol{\Psi}} \sum_{u=1}^{U} \sum_{n=1}^{\mathrm{N}} \overline{\mathcal{R}}_{sum} \tag{32a}$$

$$\text{s.t. (19b), (19c)} \tag{32b}$$

Problem 32 is still an NCOP because the objective function is complicated, and the constraint (19c) is non-convex. The NTBS 3D positions are optimized depending on the optimal RIS reflection angles and coefficients, where a 3D matrix is created to represent the NTBS 3D positions.

The optimal RIS reflection angles and coefficients, as well as the NTBS 3D positions, are obtained by invoking the MGWO algorithm, which directly determines the corresponding $\boldsymbol{r}_{u,i}$, and $\mathcal{H}^{j}_{u,i}$, respectively. The algorithm is initialized with a relatively high number of SAs and follows the steps described in algorithm 2 to reach an efficient solution. Our simulations indicate that this algorithm converges to a desirable solution after several iterations. Optimizing the RIS reflection angles, RIS reflection coefficients and the NTBS 3D positions can convert problem (19a) into a problem that can be linearly solved using $\boldsymbol{\theta}$, $\boldsymbol{\phi}$, and Ψ, respectively. We utilize a linear technique based on interference mitigation to solve $\boldsymbol{\theta}$, $\boldsymbol{\phi}$, and Ψ.

The optimization problem can be reformulated as follows:

$$\max_{\boldsymbol{\theta},\boldsymbol{\phi},\boldsymbol{\Psi}} \sum_{u=1}^{U} \sum_{n=1}^{\mathrm{N}} \overline{\mathcal{R}}_{sum} \tag{33a}$$

$$H^{j}_{u,i} = \sqrt{\frac{\mathfrak{d}}{\left\|\mathfrak{M}\Psi_j - \mathfrak{U}^{u}_{i}\right\|^{\alpha_1}}} \sqrt{\frac{1}{\beta_1+1}} \left(\sqrt{\beta_1}\bar{\mathcal{H}}^{j}_{u,i} + \tilde{\mathcal{H}}^{j}_{u,i}\right) \tag{33b}$$

$$\boldsymbol{g}_j = \vartheta \sqrt{\frac{\mathfrak{d}}{\left\|\mathfrak{M}\Psi_u - \mathfrak{q}\right\|^2}} \left[e^{-j\frac{2\pi}{\lambda}\mathfrak{r}\vartheta \frac{{}^{x}\mathfrak{q}^{-x_u}}{\left\|\mathfrak{q}-\mathfrak{M}\Psi_u\right\|}} \right]^{T} \tag{33c}$$

$$\mathcal{o} = \left| H^{j}_{u,i} + \boldsymbol{r}_{u,i}{}^{H} \mathcal{b}\boldsymbol{\vartheta}\boldsymbol{g}_j \right|^2 \tag{33d}$$

$$\overline{\mathcal{R}}_{sum} \geq \log_2 \left(1 + \frac{\mathcal{o}\mathfrak{s}^{u}_{\mathfrak{t},i}\, \mathcal{P}_{\mathfrak{t},i}}{\mathcal{o}\sum_{\mathfrak{t}=1,\mathfrak{t}\neq i}^{M_u} \mathfrak{s}^{u}_{\mathfrak{t},i} \mathcal{P}_{u,\mathfrak{t}} + \sum_{j=1,j\neq u}^{U} \mathcal{o}_j \sum_{\ell=1}^{M_j} \mathcal{P}_{j,\ell} + \sigma^2}\right) \tag{33e}$$

$$[x_{UB}, y_{UB}, z_{UB}] \geq \mathfrak{M}\boldsymbol{\Psi}_u \geq [x_{LB}, y_{LB}, z_{LB}], \forall u \in U \tag{33f}$$

$$\mathcal{b}\boldsymbol{\vartheta} = \phi_{\mathfrak{z}}.\mathrm{dia\,g}\left(\boldsymbol{\theta}_{\mathfrak{z}} * 1_{\mathrm{N}\times 1}\right) \in \mathbb{C}^{\mathrm{N}\times\mathrm{N}} \tag{33g}$$

$$\boldsymbol{\theta}_{\mathfrak{z}n} \in (0, 2\pi)\ \forall\, n \in \mathrm{N} \tag{33h}$$

$$\boldsymbol{\phi}_{\mathfrak{z}n} \in (0, 1)\, \forall n \in \mathrm{N} \tag{33i}$$

where $H^{j}_{u,i} \in \mathbb{C}^{1\times 1}$ refers to the optimal communication channel between the j^{th} NTBS and the $(u,i)^{th}$. $\boldsymbol{g}_j \in \mathbb{C}^{\mathrm{N}\times 1}$ represents the optimal communication channel between the u^{th} NTBS and the RIS. $\mathcal{o}$ is the optimal efficient power gain of the communication channel between the i^{th} NTBS and the $(u,i)^{th}$ user with the assistance of the RIS. $\boldsymbol{\theta}_{\mathfrak{z}n}$ and $\boldsymbol{\phi}_{\mathfrak{z}n}$ refer to the optimized reflection angle and reflection coefficient associated with the n^{th} sub-surface of the RIS, respectively. $\mathfrak{M}\Psi$ represents the modified 3D NTBS positions. It is obvious that the aforementioned problem is convex and can be solved utilizing meta-heuristic algorithms.

The time complexity of the suggested MGWO algorithm is $\mathcal{Q}(\mu_i \delta \mathfrak{B})$ while the time complexity of the other compared BCD [17], Greedy [30], and Annealing [32] algorithms is $\mathcal{Q}(\mu_i \dagger \wr)$, $\mathcal{Q}(\mathfrak{n}\log\mathfrak{n})$, $\mathcal{Q}\left(\mu_i \mathfrak{f}\right)$ respectively. This demonstrates that the suggested MGWO has the same time complexity as the BCD and Annealing algorithms, as well as a higher time complexity than the Greedy algorithm.

Where δ refers to the number of SAs, $\mathfrak{B}$ represents the dimension of the search space, $\dagger$ is the average complexity of optimizing each block, $\wr$ refers to the dimensionality of the sub-problem, $\mathfrak{n}$ is the number of elements or decisions to

Algorithm 1 Algorithm for the Proposed System

1) Initialize environment variables.
2) i = 0.
3) Maximum iterations = 200.
4) While i < Maximum iterations.
5) Initialize user locations randomly.
6) Set random RIS reflection angles.
7) Set RIS reflection coefficients as ones.
8) Calculate optimal RIS reflection angles according to algorithm (2).
9) Calculate optimal RIS reflection coefficients based on optimal RIS reflection angles according to algorithm (2).
10) Calculate optimal 3D position of NTBS based on user locations, optimal RIS reflection angles, and optimal RIS reflection coefficients, according to algorithm (2).
11) Calculate maximum sum rate.
12) i = ++.
13) End while.
14) Display maximum sum rate.

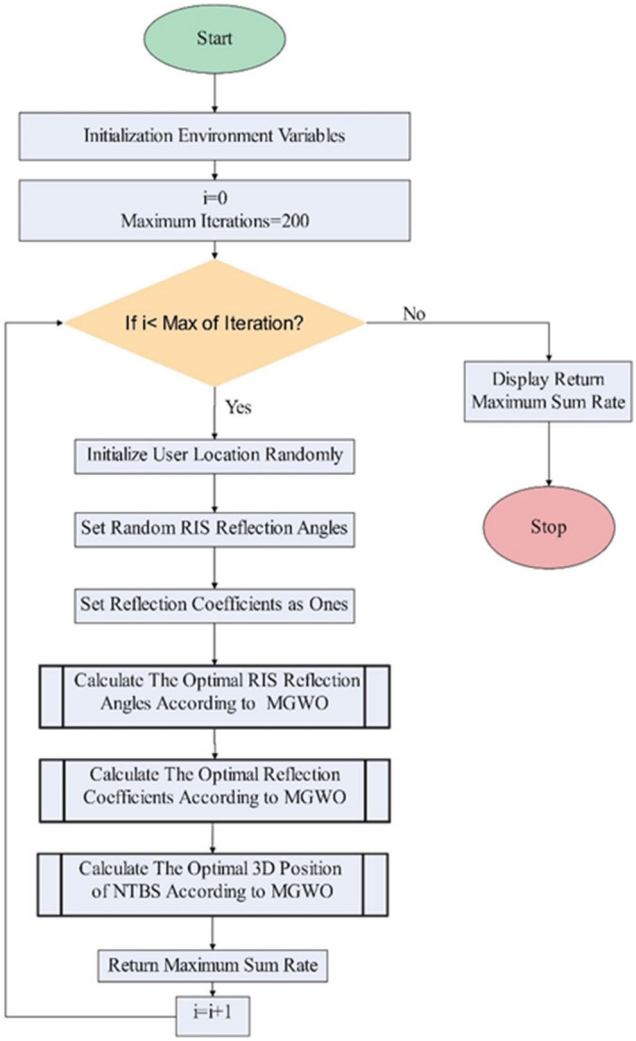

FIGURE 2. The flowchart of Algorithm 1(main function).

be made, $\mathfrak{f}$ represents the computational effort or resources required to perform a single calculation of the objective function.The flowchart of the main function and MGWO are depicted in Fig. 2 and Fig.3, respectively.

Algorithm 2 The Modified GWO Algorithm for Optimizing NTBS 3D Positions and RIS Reflection Angles and Coefficients

1) Input (Number of SAs, Maximum Iterations, Lower bound, Upper bound, Dimension, Objective function).
2) Initialize Alpha, Beta, and Delta positions.
3) Initialize the positions of SAs.
4) t = 0
5) While t < Maximum iterations.
6) For i = 1: size(positions,1)
7) Return the SAs that go beyond the boundaries of the search space.
8) Calculate the objective function for each search agent.
9) Update Alpha, Beta, and Delta positions.
10) If fitness>Alpha score
11) Update Alpha
12) End If
13) If fitness<Alpha score and fitness>Beta score
14) Update Beta
15) End If
16) If fitness<Alpha score and fitness<Beta score and fitness>Delta score
17) Update Delta
18) End If
19) End For
20) Update the position of SAs including Omega.
21) For i = 1: size(position,1)
22) For j = 1: size(position,2)
23) Calculate $\vec{c}_1^1, \vec{c}_1^2, \vec{Y}_{1o}$.
24) Calculate $\vec{c}_2^1, \vec{c}_2^2, \vec{Y}_{2o}$. According to equations (22, 27, 28)
25) Calculate $\vec{c}_3^1, \vec{c}_3^2, \vec{Y}_{3o}$.
26) Position $(\mathbf{i}, \mathbf{j}) = (\vec{Y}_{1o}, \vec{Y}_{2o}, \vec{Y}_{3o})/3$ According to eq. (29)
27) End For
28) End For
29) t = t + 1
30) Convergence curve (t) = Alpha score
31) End While
32) Return the best feasible solution vector of reflection angles, reflection coefficients, and NTBS 3D position values.

V. NUMERICAL RESULTS AND DISCUSSION

A. ASSUMPTIONS OF THE SIMULATION

The behavior of the proposed RIS-based NOMA HetNet is assessed in this study, which is achieved through simulation of its performance, and compares it with traditional algorithms such as BCD, Annealing, Greedy, GWO OMA, NOMA+RIS, and NOMA-RIS. We consider a network with U = 2 NTBSs serving 2 user clusters. Each cluster comprises 2 GUs that have a random and uniform distribution in two neighboring areas of 100 × 100 m^2. The results were obtained using one random realization of the distributions of GUs, as demonstrated in Fig. 4. The parameters used in the simulation are defined as follows: The RIS is positioned at coordinates (100, 50, 20) meters, and the number of sub-surfaces in the RIS element is set to $\mathcal{N} = 20$. The PLEs and Rician fading channel factors for both the NTBS-user link and the RIS-user are assigned the same values. Expressly, the PLEs are set to $\alpha_1 = \alpha_2 = 2.9$, and the Rician factors are set to $\beta_1 = \beta_2 = 10$ dB. NTBSs are permitted to fly at a maximum altitude of 100 meters and a minimum altitude of 60 meters. To simplify the scenario, we suppose that all NTBSs possess the same maximum transmission power, which can be denoted as $p_{max,u} = p_{max} = 20$dB, $\forall u \in U$.

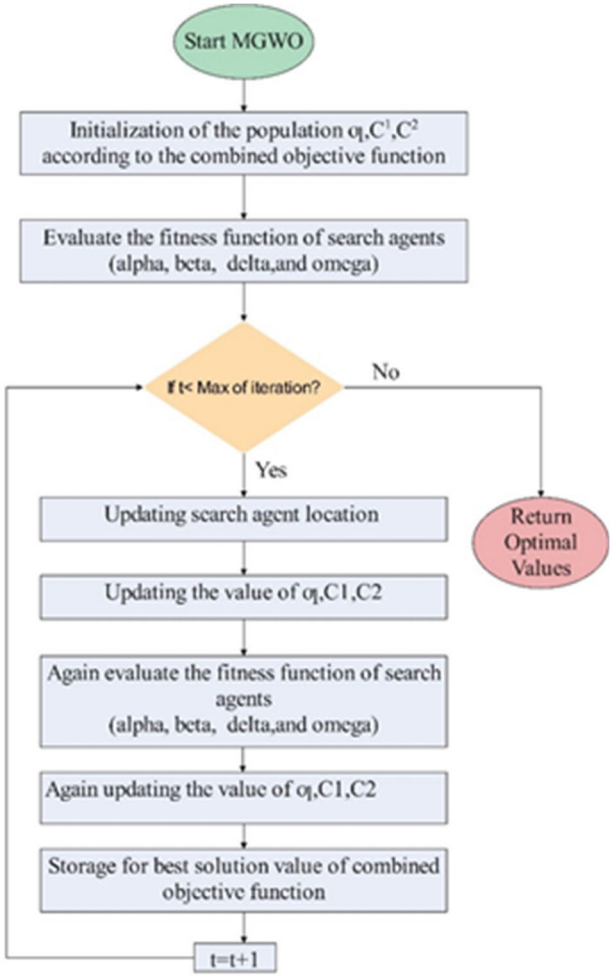

FIGURE 3. The flowchart of Algorithm 2 (MGWO).

During the first step of each initialization, the horizontal positions of NTBSs are produced uniformly and randomly in each area of 100 x 100 m^2. The initial flying height is set to $z_u = Z_{max} + Z_{min}/2$, $\forall u \in U$. Second, the MGWO is used to determine the optimal NTBS 3D positions. After that, the NOMA-SIC among GUs in each cluster is established depending on the distances of the GUs to the paired NTBSs. The maximum transmission power is assigned to each NTBS and distributed equally among all GUs served by that NTBS. Each RIS sub-surface's reflection angle and reflection coefficient are randomly and uniformly produced in the range of $[0, 2\pi]$ and [0, 1], respectively.

B. RESULTS AND DISCUSSION

Fig. 5 illustrates the SSR plotted concerning the signal-to-noise ratio (SNR) for the proposed algorithm in comparison with conventional algorithms such as BCD, Annealing, Greedy, GWO OMA, NOMA+RIS, and NOMA-RIS. As the SNR increases, the proposed algorithm achieves a higher SSR than BCD, Annealing, Greedy, GWO OMA, NOMA+RIS, and NOMA-RIS. This is because optimizing the IRS

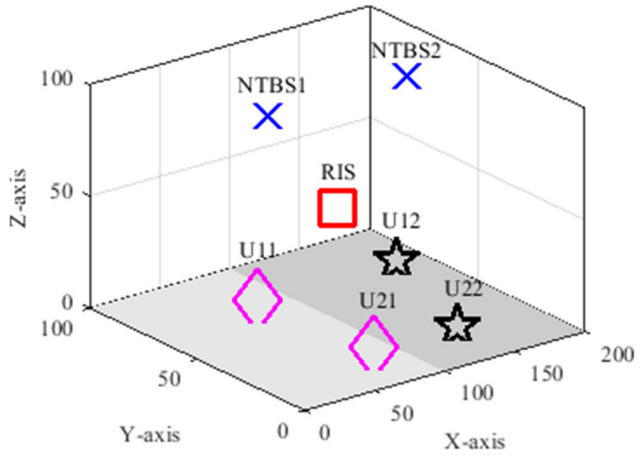

FIGURE 4. The simulations' network topology.

reflection angles, coefficients, and NTBS 3D positions greatly impacts interference mitigation. The results state that the suggested algorithm notably impacts the SSR increment. It is clear that with the increase of the SNR from 0 to 100 dBm, the SSR of BCD, Annealing, Greedy, NOMA+RIS, NOMA-RIS, and GWO OMA stabilized at 6.501, 5.286, 5.014, 4.741, 4.723, and 3.344 bits/s/Hz, respectively. The best SSR is achieved in the case of the proposed method with 7.443 bits/s/Hz. From Fig. 5 we also see that both the NOMA+RIS and NOMA-RIS schemes have very close SSR values.

These significant improvements to the SSR can be explained by the fact that the GWO's principal work in solving such problems is more accurate than that of other traditional algorithms, which means the GWO works more accurately to reach the ideal value. Moreover, the MGWO minimizes the distance between the wolves and their prey and enhances the search process's precision, as explained in equations 27a, 27b, and 27c.

At different numbers of sub-surfaces, the SSR for the proposed algorithm in comparison with BCD, Annealing, Greedy, GWO OMA, NOMA+RIS, and NOMA-RIS is depicted in Fig. 6. When the number of sub-surfaces is 20, the SSR for NOMA+RIS, Greedy, BCD, Annealing, GWO OMA, and the proposed RIS-enhanced multi-NTBS NOMA networks is equal to 4.02, 4.04, 4.66, 4.98, 7.30, and 8.74 bits/s/Hz, respectively. Increasing the number of sub-surfaces to 80 increases these values to 4.06, 4.07, 8.48, 7.16, 10.01, and 11.48 bits/s/Hz, respectively. These results are because increasing the number of sub-surfaces can improve the SSR by increasing the number of reflecting paths and enhancing the diversity gain. However, in the NOMA-RIS scheme, the achieved SSR is not affected by the variation of the number of sub-surfaces, which confirms the advantages of the RIS.

The proposed algorithm attains a higher SSR performance among all the aforementioned algorithms. This is due to the fact that the NOMA permits the simultaneous service of all

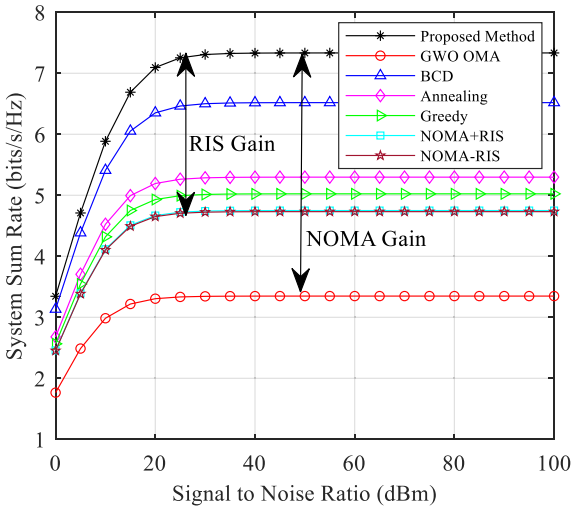

FIGURE 5. The performance of the suggested system, BCD [17], Greedy [30], Annealing [32], GWO OMA, NOMA+ RIS, and NOMA-RIS concerning the SSR at various SNR values.

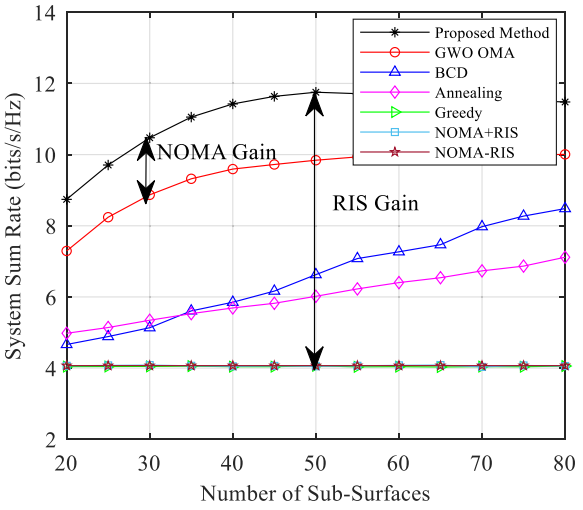

FIGURE 6. The performance of the proposed system, BCD [17], Greedy [30], Annealing [32], GWO OMA, NOMA+RIS, and NOMA-RIS regarding the SSR at different numbers of sub-surfaces.

users in all resource blocks (RBs), thereby enabling flexible RAs that enhance SE. Moreover, optimizing the NTBS 3D positions as well as the reflection angles and coefficients of RIS introduces a new degree of freedom for implementing NOMA by designing the decoding order through the NTBS 3D positions and mitigating inter-group interference by adjusting IRS reflection angles and coefficients. As aforementioned, the distribution of GUs is random and uniform, resulting in different user locations at each iteration. This affects the communication channels between the NTBS and the GUs, as well as the communication channels between the RIS and the GUs, which in turn affects the calculation of the system sum rate. Compared to NOMA, OMA has the worst performance because it allocates a limit of RBs for each GU. We also noticed that RIS has a much higher gain for NOMA than the other schemes mentioned above.

The effect of variations in the SNR versus the system EE is illustrated in Fig. 7. The numerical results indicate that the system EE increases as the SNR increases throughout all seven schemes. This is due to the fact that as SNR increases, the total sum rate of the proposed system also increases. Also, the results show that the proposed algorithm has substantially improved the performance of the system EE. This is due to the SIC decoding order among GUs for the proposed system, which results in much more EE gain compared with other schemes. It is clear that with an increase in the SNR from 0 to 100 dBm, the system EE of BCD, Annealing, Greedy, NOMA-RIS, NOMA+RIS, and GWO OMA stabilized at 125.112, 98.64, 85.114, 84.081, 82.454, and 34.140 bits/joule, respectively. Moreover, the SSR for the proposed method reaches 157.648 bit/joule.

Fig. 8 plots the SSR for seven cases versus the PLE. These results clearly illustrate the impact of the PLE on the sum rate, considering that both the power and the SNR of NTBS are constant. When the PLE is 2, the SSR for the cases

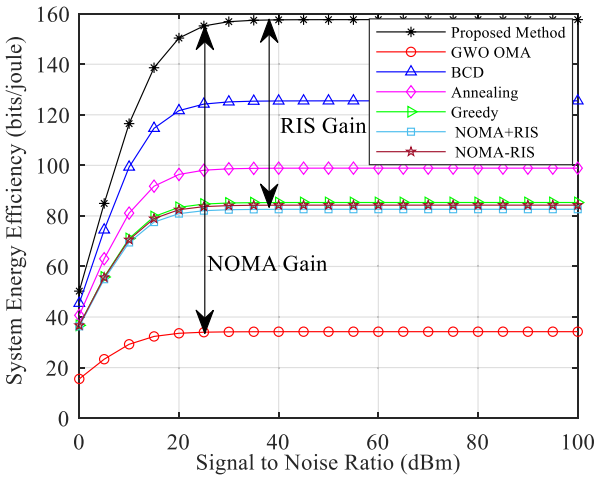

FIGURE 7. The performance of the proposed system, BCD [17], Greedy [30], Annealing [32], GWO OMA, NOMA+RIS, and NOMA-RIS concerning EE at various SNR values.

NOMA-RIS, Greedy, NOMA+RIS, BCD, Annealing, GWO OMA, and the proposed RIS-enhanced multi-NTBS NOMA is equal to 1.173, 1.205, 1.266, 1.882, 2.153, 2.520, and 3.754 bits/s/Hz, respectively. Increasing the PLE to 4 leads to a decrease in these values to 0.723, 0.739, 0.774, 1.108, 1.004, 1.655, and 2.354 bits/s/Hz, respectively. These results can be explained by the fact that as the PLE increases, a more significant attenuation of the signal with distance is achieved, leading to a decrease in the SSR. Moreover, the IRS's reflecting signal weakens when the PLE of the RIS-GU link increases. Therefore, an increase in the PLE value can cause a significant reduction in the coverage area and the maximum achievable communication range, making it more challenging to maintain reliable communication links with the NTBS.

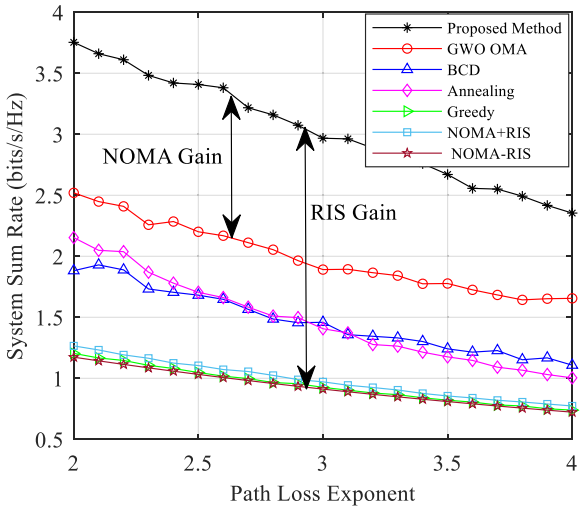

FIGURE 8. The performance of the suggested system, BCD [17], Greedy [30], Annealing [32], GWO OMA, NOMA+RIS, and NOMA-RIS regarding the SSR at various values of PLE.

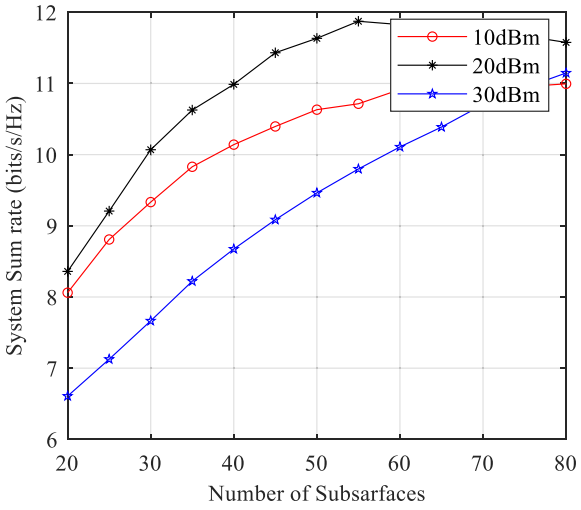

FIGURE 10. The performance of the suggested system with various maximum power requirements regarding SSR at different numbers of sub-surfaces.

Fig. 9 demonstrates the SSR versus SNR for different minimum QoS requirements. It is clear from the results that with an increase in the SNR from 0 to 100 dBm, while keeping the number of sub-surfaces constant, the SSR for the cases of 200, 300, 400, and 500 Kbps minimum QoS is stabilized at 2.484, 1.625, 0.716, and 0.163 bits/s/Hz, respectively. Moreover, the SSR with a 100 Kbps minimum QoS reaches 4.514 bits/s/Hz. The results stated that the highest SSR is attained when the minimum QoS is 100 kbps. Note that these values are achieved for SNR of 40 dBm and above since they remain constants with the increment of the SNR. This is because when the minimum QoS decreases, the number of user connections will increase, thereby increasing the sum rate of the proposed system.

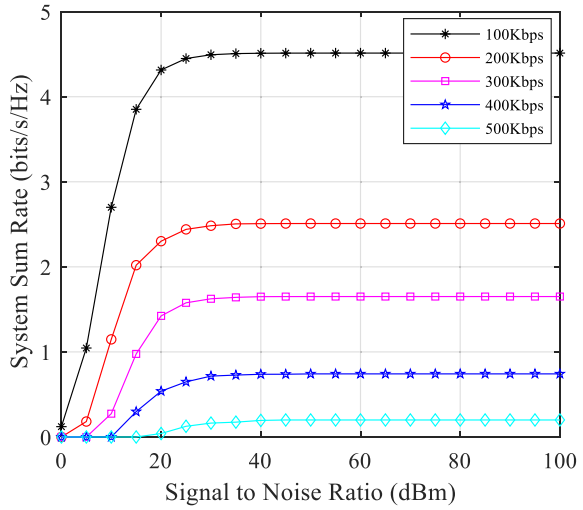

FIGURE 9. The performance of the proposed system with different minimum QoS requirements regarding the SSR at different SNR values.

The sum rate of the suggested system against the number of sub-surfaces for different NTBS maximum power transmissions is depicted in Fig. 10. It is obvious from the results that the $P_{\max}$ of NTBS plays a crucial role in aerial communication scenarios. The simulation results state that increasing the number of sub-surfaces from 20 to 80 leads to an increase in the SSR from 8.061 to 10.994 dBm when Pmax = 10, from 8.359 to 11.576 dBm when Pmax = 20, and from 6.607 to 11.147 when Pmax = 30. The NTBS power of 20 dBm is operating at an optimal level, providing sufficient power for communication while avoiding excessive interference and power consumption and overcoming noise and attenuation. While the NTBS power of 10 dBm results in weaker signals and reduced coverage. The NTBS power of 30 dBm introduces more interference and signal distortion. Furthermore, it is also clear from the results that if the number of sub-surfaces is 75 or above, the performance of 30 dBm becomes better than 10 dBm. The reason is that increasing the number of sub-surfaces requires increasing the power level to extend coverage and improve connectivity without introducing excessive interference.

In Fig. 11, the sum rate of the proposed system is plotted against the SNR with different GUs per cluster. The results show that when the SNR increases from 0 up to 12 dBm, the proposed algorithm in the case of 20 GUs per cluster, achieves a higher SSR than 10, 30, 40, and 50 GUs per cluster. When the value of SNR increases above 15 dBm, the proposed algorithm in the case of 30 GUs per cluster, achieves a higher SSR in comparison with 10, 20, 40, and 50 GUs per cluster. Furthermore, the cases of 40 and 50 GUs per cluster have an identical SSR. It is clear that when increasing the number of GUs per cluster by more than 30, the aggregate sum rate decreases. This is because when the number of GUs per cluster increases up to a specific limit, the SIC among the GUs cannot work correctly, potentially leading to higher levels of intra-cluster interference.

At various values of sub-surface, the sum rate of the proposed system with different iterations of the proposed

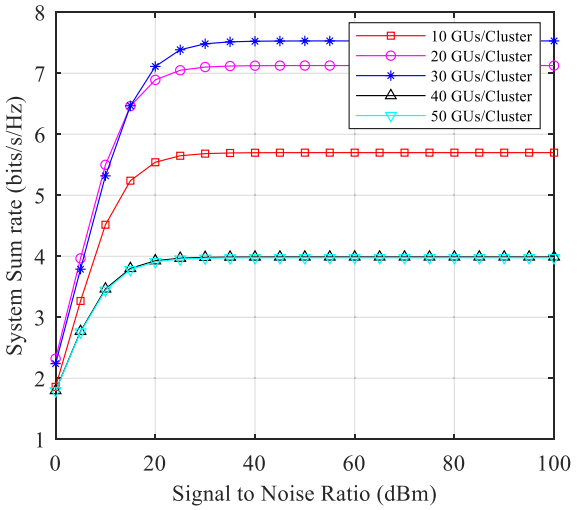

FIGURE 11. The performance of the suggested system with various GUs per cluster in terms of SSR at different SNR values.

algorithm is plotted in Fig. 12. Increasing the number of sub-surfaces from 20 to 80 while keeping the power of NTBS and SNR constant leads to an increase in the sum rate of the system for the cases of 5, 25, 50, 75, and 100 iterations by 10.799%, 21.195%, 30.756%, 36.860%, and 42.110%, respectively. The results demonstrate that the sum rate of the system increases when the number of iterations increases. This is because of the iterative nature of the optimization process, where the proposed algorithm continuously refines and updates the solutions over multiple iterations to converge toward an optimal solution. Overall, the increasing SSR with an increasing number of iterations in the proposed optimization algorithm can be attributed to the algorithm's ability to explore the solution space effectively and converge towards better solutions over time.

In Fig. 13, the results provide vital insight into the effect of the SAs on the performance of the SSR, particularly concerning the number of sub-surfaces and SSR using RIS with optimized reflection angles and coefficients, as well as the optimization of the 3D position of NTBSs. The observed trend, in which the aggregate rate increases as the number of SAs increases with different numbers of sub-surfaces, suggests that the number of SAs plays a crucial role in the proposed optimization algorithm. The simulation results state that by increasing the number of sub-surfaces from 20 to 80, the sum rate in the case of 10, 20, 30, 40, and 50 SAs is increased by 10.912%, 17.727%, 23.383%, 28.162%, 31.881% respectively. The results prove that these values are increasing exponentially. The reason for these results is that, on the one hand, increasing the number of sub-surfaces results in increasing the reflection paths. This increased number of reflection paths enables the RIS to create more diverse and optimized channel conditions, improving signal quality and enhancing communication links between the NTBS and GUs. On the other hand, increasing the number of SAs can accelerate the convergence of the proposed optimization algorithm towards optimal solutions. The SSR increases as the number of SAs in the proposed algorithm increases. This is because more SAs lead to better exploration, diversity, exploitation, and convergence.

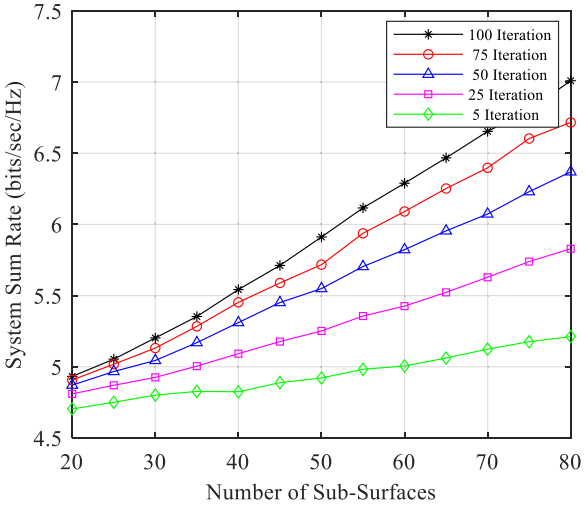

FIGURE 12. The performance of the proposed system with different iterations of the proposed algorithm in terms of SSR at various numbers of sub-surfaces.

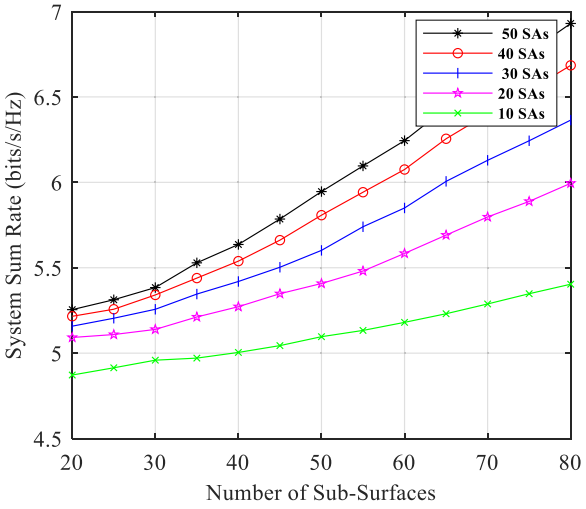

FIGURE 13. The performance of the proposed system with different SAs of the proposed algorithm in terms of SSR at various numbers of sub-surfaces.

The SSR with different iterations of the proposed algorithm versus various SNR values is plotted in Fig. 14. As the value of SNR increases from 0 to 100 dBm, the proposed algorithm with the case of 100 iterations achieves a higher SSR in comparison with that of 75, 50, 25, and 5 iterations. When the SNR is 0, the SSR for the cases of 5, 25, 50, 75, and 100 iterations is equal to 1.341, 1.449, 1.667, 1.452, and 1.744 bits/s/Hz, respectively. Increasing the SNR to 100 increases these values to 2.399, 4.167, 4.385, 4.914, and 5.067 bits/s/Hz, respectively. The results show that increasing the number of iterations of the proposed

algorithm notably impacts the SSR increment. This is because increasing SNR leads to fewer transmission errors and higher data rates. Thereby, the optimization process of the proposed algorithm becomes more effective. This implies that the proposed algorithm can better distinguish between good and poor solutions, allowing it to converge more quickly towards an optimal solution that maximizes the SSR.

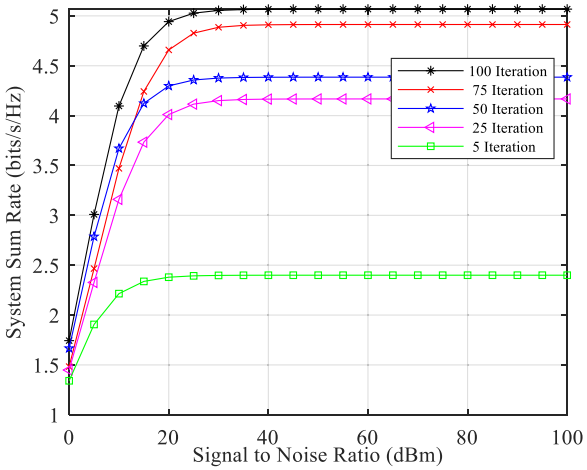

FIGURE 14. The performance of the proposed system with different iterations of the proposed algorithm regarding total sum rate at various SNR values.

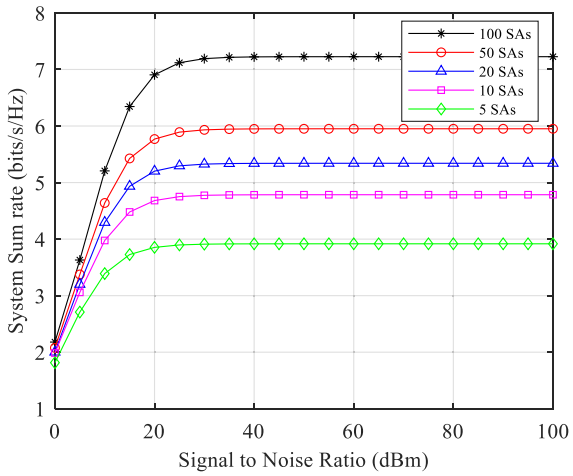

FIGURE 15. The performance of the proposed system with SAs of the proposed algorithm in terms of SSR at various values of SNR.

TABLE 1. Table of abbreviations.

Abbreviation	Full Form
A2G	Air-to-ground
ABV	Active Beamforming Vectors
AO	Alternating Optimization
ASM	Alternative Search Method
B5G	Beyond Fifth Generation
BCD	Block Coordinate Descent
CAHWOA	Chaotic Adaptative Hybrid Whale Optimization Algorithm
D2D	Device-to-Device
DL	Downlink
EE	Energy Efficiency
GUs	Ground Users
GWO	Gray Wolf Optimization
HetNets	Heterogeneous Networks
ICI	Inter-Cell Interference
IoT	Internet of Things
IRS	Intelligent Reflecting Surface
LoS	Line-of-Sight
MGWO	Modified Gray Wolf Optimization
NCOP	Non-Convex Optimization Problem
NOMA	Non-Orthogonal Multiple Access
NTBS	Non-Terrestrial Base Station
OFDMA	Orthogonal Frequency Division Multiple Access
OMA	Orthogonal Multiple Access
PA	Power Allocation
PLEs	Path Loss Exponents
PSO	particle swarm optimization
QoS	Quality of Service
RA	Resource Allocation
RIS	Reconfigurable Intelligent Surface
SA	Simulated Annealing
SCA	Successive Convex Approximation
SCMA	Sparse Code Multiple Access
SDP	Semi-Definite Programming
SDR	Semi-Definite Relaxation
SE	Spectrum Efficiency
SIC	Successive Interference Cancellation
SNR	Signal-to-Noise Ratio
SRMA	Splitting-Rate Multiple Access
SSR	System Sum Rate
STAR	Simultaneous Transmission and Reflection
SWIPT	Simultaneous Wireless Information and Power Transfer
TDMA	Time Division Multiple Access
TRC	Transmission and Reflection Coefficients
UAV	Unmanned Aerial Vehicles
UL	Uplink

The crucial insights into the impact of search agent performance on the SSR are presented in Fig. 15, specifically concerning the SNR and the SSR. The observed trend that the aggregate rate increases as the number of SAs with different SNR values increases shows that the number of SAs significantly affects the proposed optimization algorithm. It is clear from the results that with an increase in the SNR, while keeping the number of sub-surfaces constant, the SSR for the cases of 5, 10, 20, and 50 SAs is stabilized at 3.910, 4.774, 5.326, and 5.932 bits/s/Hz, respectively. Moreover, the SSR with 100 SAs reaches 7.226 bits/s/Hz. These results are because with increased SNR values and the number of SAs, the proposed algorithm can converge to optimal solutions more quickly. The higher SNR reduces the complexity of the optimization problem, making it easier for the algorithm to converge. Additionally, increasing the number of SAs accelerates the exploration of the solution space, facilitating quicker convergence toward optimal solutions. This faster convergence results in an increase in the sum rate of the proposed system.

VI. CONCLUSION AND FUTURE WORKS

In this paper, we employ RIS-aided NTBSs with NOMA in DL HetNets. The SSR and EE maximization for the proposed system is achieved by the joint optimization of NTBS 3D positions, RIS reflection angles, RIS reflection coefficients, and SIC among GUs. Moreover, an MGWO-based meta-heuristic algorithm is proposed to address the formulated non-convex optimization problem. In particular, the original optimization problem is divided into three sub-problems (i.e., RIS reflection angles, RIS reflection coefficients, and NTBS 3D position), which are then addressed alternately using the proposed optimization technique. Our simulation results stated that the suggested algorithm is found to be able to increase the SSR and EE significantly in comparison with the conventional schemes. The results also showed that using the RIS with random reflection angles has the same effect on performance as without the RIS. This highlights the significance of optimizing the coefficients and reflection angles of the RIS in communication networks based on RIS. Moreover, integrating RIS with NTBS in DL HetNets is efficient in enhancing the total system performance by improving the channel quality between NTBSs and their respective GUs while minimizing inter-NTBS interference. Future research includes incorporating NTBS PA optimization into the joint optimization process and accounting for multiple RISs.

ABBREVIATIONS

See Table 1.

REFERENCES

[1] O. T. H. Alzubaidi, M. N. Hindia, K. Dimyati, K. A. Noordin, A. N. A. Wahab, F. Qamar, and R. Hassan, "Interference challenges and management in B5G network design: A comprehensive review," *Electronics*, vol. 11, no. 18, p. 2842, Sep. 2022.

[2] H. F. Alhashimi, M. N. Hindia, K. Dimyati, E. B. Hanafi, N. Safie, F. Qamar, K. Azrin, and Q. N. Nguyen, "A survey on resource management for 6G heterogeneous networks: Current research, future trends, and challenges," *Electronics*, vol. 12, no. 3, p. 647, Jan. 2023.

[3] O. H. Al-Zubaidi, R. Paulus, A. Jaiswal, A. Ashok, and A. Shukla, "Analysis of QoS for WiMAX and 3G networks with same and different speed using QualNet 6.1," *IOSR J. Electron. Commun. Eng.*, vol. 9, no. 1, pp. 131–138, Feb. 2012.

[4] W. Khawaja, I. Guvenc, D. W. Matolak, U.-C. Fiebig, and N. Schneckenburger, "A survey of air-to-ground propagation channel modeling for unmanned aerial vehicles," *IEEE Commun. Surveys Tuts.*, vol. 21, no. 3, pp. 2361–2391, 3rd Quart., 2019.

[5] F. B. Mismar and A. O. Kaya, "Uncoordinated interference avoidance between terrestrial and non-terrestrial communications," 2023, *arXiv:2304.07129*.

[6] W. Shin, M. Vaezi, B. Lee, D. J. Love, J. Lee, and H. V. Poor, "Non-orthogonal multiple access in multi-cell networks: Theory, performance, and practical challenges," *IEEE Commun. Mag.*, vol. 55, no. 10, pp. 176–183, Oct. 2017.

[7] W. Shin, M. Vaezi, B. Lee, D. J. Love, J. Lee, and H. V. Poor, "Coordinated beamforming for multi-cell MIMO-NOMA," *IEEE Commun. Lett.*, vol. 21, no. 1, pp. 84–87, Jan. 2017.

[8] B. Rana, S.-S. Cho, and I.-P. Hong, "Review paper on hardware of reconfigurable intelligent surfaces," *IEEE Access*, vol. 11, pp. 29614–29634, 2023.

[9] M. Abdelrahman, A. Nasser, A. Magdy, and M. Elsabrouty, "Multi-armed bandit based capacity enhancement approach for reconfigurable intelligent surface assisted multi-cell system," in *Proc. 10th Int. Jpn.-Africa Conf. Electron., Commun., Computations (JAC-ECC)*, Dec. 2022, pp. 72–75.

[10] W. U. Khan, E. Lagunas, A. Mahmood, Z. Ali, M. Asif, S. Chatzinotas, and B. Ottersten, "Integration of NOMA with reflecting intelligent surfaces: A multi-cell optimization with SIC decoding errors," *IEEE Trans. Green Commun. Netw.*, vol. 7, no. 3, pp. 1554–1565, Mar. 2023.

[11] H. Zhou, M. Erol-Kantarci, Y. Liu, and H. Vincent Poor, "Heuristic algorithms for RIS-assisted wireless networks: Exploring heuristic-aided machine learning," 2023, *arXiv:2307.01205*.

[12] A. Nasser, O. Elnahas, O. Muta, and Z. Quan, "Data-driven spectrum allocation and power control for NOMA HetNets," *IEEE Trans. Veh. Technol.*, vol. 72, no. 9, pp. 11685–11697, Apr. 2023.

[13] H. F. Alhashimi, M. N. Hindia, K. Dimyati, E. B. Hanafi, and T. F. T. M. N. Izam, "Joint optimization scheme of user association and channel allocation in 6G HetNets," *Symmetry*, vol. 15, no. 9, p. 1673, Aug. 2023.

[14] F. Qamar, A. Gachhadar, S. H. A. Kazmi, and R. Hassan, "Success probability and spectral efficiency estimation using successive interference cancellation for B5G network," in *Proc. IEEE Int. Conf. Comput. (ICOCO)*, Oct. 2023, pp. 213–218.

[15] F. Qamar, A. Gachhadar, S. H. Ali Kazmi, and R. Hassan, "Successive interference cancellation approach to estimated outage and coverage probability for UDN B5G network," in *Proc. IEEE Int. Conf. Artif. Intell. Eng. Technol. (IICAIET)*, Sep. 2023, pp. 182–187.

[16] D. Mohamed, A. Magdy, O. Elghandour, and A. Nasser, "Data-driven based algorithm for joint HetNets power allocation and NOMA user pairing," in *Proc. 10th Int. Jpn.-Africa Conf. Electron., Commun., Comput. (JAC-ECC)*, Dec. 2022, pp. 94–97.

[17] X. Mu, Y. Liu, L. Guo, J. Lin, and H. V. Poor, "Intelligent reflecting surface enhanced multi-UAV NOMA networks," *IEEE J. Sel. Areas Commun.*, vol. 39, no. 10, pp. 3051–3066, Oct. 2021.

[18] W. Feng, J. Tang, Q. Wu, Y. Fu, X. Zhang, D. K. C. So, and K.-K. Wong, "Resource allocation for power minimization in RIS-assisted multi-UAV networks with NOMA," *IEEE Trans. Commun.*, vol. 71, no. 11, pp. 6662–6676, Nov. 2023.

[19] M. Hadi and R. Ghazizadeh, "Computation bits enhancement for IRS-assisted multi-UAV wireless powered mobile edge computing systems," *Veh. Commun.*, vol. 43, Oct. 2023, Art. no. 100656.

[20] H. Peng, Y. Zheng, P. He, Y. Cui, R. Wang, and D. Wu, "Reliability optimization in IRS-assisted UAV networks," *Veh. Commun.*, vol. 44, Dec. 2023, Art. no. 100679.

[21] H. Zhao, Z. Kong, H. Huang, S. Shi, Y. Ni, G. Gui, H. Gacanin, H. Sari, and F. Adachi, "Air reconfigurable intelligent surface enhanced multi-user NOMA system," *IEEE Internet Things J.*, vol. 11, no. 1, pp. 29–39, May 2023.

[22] Y. Liu, W. Chen, H. Tang, and K. Wang, "Resource allocation in the RIS assisted SCMA cellular network coexisting with D2D communications," *IEEE Access*, vol. 11, pp. 39978–39989, 2023.

[23] M. Asif, A. Ihsan, W. U. Khan, Z. Ali, S. Zhang, and S. X. Wu, "Energy-efficient beamforming and resource optimization for STAR-IRS enabled hybrid-NOMA 6G communications," *IEEE Trans. Green Commun. Netw.*, vol. 7, no. 3, pp. 1356–1368, Sep. 2023.

[24] G. Grieco, G. Iacovelli, D. Pugliese, D. Striccoli, and L. A. Grieco, "A system-level simulation module for multi-UAV IRS-assisted communications," 2023, *arXiv:2304.00929*.

[25] B. Shi, Y. Wang, D. Li, W. Cai, J. Lin, S. Zhang, W. Shi, S. Yan, and F. Shu, "STAR-RIS-UAV-Aided coordinated multipoint cellular system for multi-user networks," *Drones*, vol. 7, no. 6, p. 403, Jun. 2023.

[26] X. Zhang, H. Zhang, W. Du, K. Long, and G. K. Karagiannidis, "Joint resource allocation and reflecting design in IRS-UAV communication networks with SWIPT," *IEEE Trans. Wireless Commun.*, vol. 23, no. 4, pp. 2533–2546, Apr. 2024.

[27] J. Zhao, L. Yu, K. Cai, Y. Zhu, and Z. Han, "RIS-aided ground-aerial NOMA communications: A distributionally robust DRL approach," *IEEE J. Sel. Areas Commun.*, vol. 40, no. 4, pp. 1287–1301, Apr. 2022.

[28] N. T. Nguyen, V.-D. Nguyen, H. Van Nguyen, Q. Wu, A. Tölli, S. Chatzinotas, and M. Juntti, "Fairness enhancement of UAV systems with hybrid active-passive RIS," *IEEE Trans. Wireless Commun.*, vol. 23, no. 5, pp. 4379–4396, May 2024.

[29] W. Jiang, B. Ai, M. Li, W. Wu, and X. Shen, "Average age of information minimization in aerial IRS-assisted data delivery," *IEEE Internet Things J.*, vol. 10, no. 17, pp. 15133–15146, Apr. 2023.

[30] S. Chen, F. Liu, and Y. Liu, "Sum rate maximization for intelligent reflecting surface-assisted UAV-enabled NOMA network," *Electronics*, vol. 12, no. 17, p. 3616, Aug. 2023.

[31] S. K. Singh, K. Agrawal, K. Singh, B. Clerckx, and C.-P. Li, "RSMA for hybrid RIS-UAV-aided full-duplex communications with finite block-length codes under imperfect SIC," *IEEE Trans. Wireless Commun.*, vol. 22, no. 9, pp. 5957–5975, Jan. 2023.

[32] D. Wang, X. Li, Y. He, F. Zhou, and Q. Wu, "Intelligent reflecting surface assisted untrusted NOMA transmissions: A secrecy perspective," *Sci. China Inf. Sci.*, vol. 66, no. 9, Sep. 2023, Art. no. 192302.

[33] N. Hamden, A. Nasser, M. Y. Selim, and M. Elsabrouty, "Reinforcement learning based technique for interference management in UAV aided HetNets," in *Proc. 10th Int. Jpn.-Africa Conf. Electron., Commun., Comput. (JAC-ECC)*, Dec. 2022, pp. 81–84.

[34] T. Naous, M. Itani, M. Awad, and S. Sharafeddine, "Reinforcement learning in the sky: A survey on enabling intelligence in NTN-based communications," *IEEE Access*, vol. 11, pp. 19941–19968, 2023.

[35] L. Zhang, J. Liu, M. Sheng, N. Zhao, and J. Li, "Exploiting collaborative computing to improve downlink sum rate in satellite integrated terrestrial networks," *IEEE Trans. Veh. Technol.*, vol. 72, no. 4, pp. 4670–4682, Apr. 2023.

[36] S. Li, B. Duo, X. Yuan, Y.-C. Liang, and M. Di Renzo, "Reconfigurable intelligent surface assisted UAV communication: Joint trajectory design and passive beamforming," *IEEE Wireless Commun. Lett.*, vol. 9, no. 5, pp. 716–720, May 2020.

[37] C. Zhang, W. Yi, Y. Liu, K. Yang, and Z. Ding, "Reconfigurable intelligent surfaces aided multi-cell NOMA networks: A stochastic geometry model," *IEEE Trans. Commun.*, vol. 70, no. 2, pp. 951–966, Feb. 2022.

[38] A. M. Huroon, Y.-C. Huang, and L.-C. Wang, "UAV-RIS assisted multiuser communications through transmission strategy optimization: GBD application," *IEEE Trans. Veh. Technol.*, vol. 73, no. 6, pp. 8584–8597, Feb. 2024.

[39] Q. Wu and R. Zhang, "Towards smart and reconfigurable environment: Intelligent reflecting surface aided wireless network," *IEEE Commun. Mag.*, vol. 58, no. 1, pp. 106–112, Jan. 2020.

[40] A. Nasser, O. Muta, M. Elsabrouty, and H. Gacanin, "Interference mitigation and power allocation scheme for downlink MIMO–NOMA HetNet," *IEEE Trans. Veh. Technol.*, vol. 68, no. 7, pp. 6805–6816, Jul. 2019.

[41] A. M. H. Alibraheemi, M. N. Hindia, K. Dimyati, T. F. T. M. N. Izam, J. Yahaya, F. Qamar, and Z. H. Abdullah, "A survey of resource management in D2D communication for B5G networks," *IEEE Access*, vol. 11, pp. 7892–7923, 2023.

[42] A. Nasser, O. Muta, M. Elsabrouty, and H. Gacanin, "Compressive sensing based spectrum allocation and power control for NOMA HetNets," *IEEE Access*, vol. 7, pp. 98495–98506, 2019.

[43] S. Mirjalili, S. M. Mirjalili, and A. Lewis, "Grey wolf optimizer," *Adv. Eng. Softw.*, vol. 69, pp. 46–61, Mar. 2014.

[44] S. K. Goudos, P. D. Diamantoulakis, A. D. Boursianis, P. Sarigiannidis, K. E. Psannis, M. A. Matin, S. Wan, and G. K. Karagiannidis, "Joint QoS aware admission control and power allocation in NOMA downlink networks," *IEEE Access*, vol. 11, pp. 30873–30887, 2023.

OSAMAH THAMER HASSAN ALZUBAIDI received the B.E. degree in communication techniques from Al-Furat Al-Awsat Technical University, Najaf, Iraq, in 2011, and the Master of Technology degree in electronics and communication engineering (communication system engineering) from SHIATS University, Allahabad, India, in 2014. He is currently pursuing the Ph.D. degree in electrical engineering (major in wireless communication) with the Faculty of Engineering, University of Malaya, Kuala Lumpur, Malaysia. He has more than ten years of research and teaching experience. His research interests include wireless networks, interference management, NTBS communication, NOMA communication, and RIS communication for B5G.

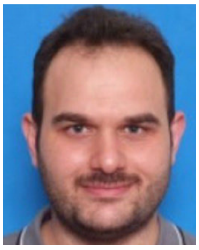

MHD NOUR HINDIA (Member, IEEE) received the Ph.D. degree from the Faculty of Engineering in Telecommunication, University of Malaya, Kuala Lumpur, Malaysia, in 2015. He is currently involved with research in the field of wireless communications, especially in channel sounding, network planning, converge estimation, handover, scheduling, and quality of service enhancement for 5G networks. He is currently a Postdoctoral Fellow with the Faculty of Engineering in Telecommunication, University of Malaya. Besides that, he is involved with research with the Research Group in Modulation and Coding Scheme for Internet of Things for Future Network. He has authored or coauthored a number of science citation index journals and conference papers. He has participated as a reviewer and a committee member of a number of ISI journals and conferences.

KAHARUDIN DIMYATI (Member, IEEE) received the degree from the University of Malaya, Malaysia, in 1992, and the Ph.D. degree from the University of Wales, Swansea, U.K., in 1996. He is currently a Professor with the Department of Electrical Engineering, Faculty of Engineering, University of Malaya. Since joining the university, he is actively involved in teaching, postgraduate supervision, research, and administration. To date, he has supervised 15 Ph.D. students and 32 master's students by research students. He has published over 100 journal articles. He is also a member of IET and IEICE. He is also a Professional Engineer and a Chartered Engineer.

KAMARUL ARIFFIN NOORDIN (Senior Member, IEEE) received the B.Eng. (Hons.) and M.Eng. degrees from the University of Malaya, Kuala Lumpur, Malaysia, in 1998 and 2001, respectively, and the Ph.D. degree in communication systems from Lancaster University, U.K., in 2009. He is currently an Associate Professor with the Department of Electrical Engineering, University of Malaya. His research interests include resource allocation in wireless networks, cognitive radio networks, device-to-device communications, network modeling, and performance analysis.

FAIZAN QAMAR (Member, IEEE) received the B.E. degree in electronics from Hamdard University, Karachi, Pakistan, in 2010, the M.E. degree in telecommunication from NED University, Karachi, in 2013, and the Ph.D. degree in wireless networks from the Faculty of Engineering, University of Malaya, Kuala Lumpur, Malaysia, in October 2019. He is currently a Senior Lecturer with the Faculty of Information Science and Technology, Universiti Kebangsaan Malaysia [The National University of Malaysia (UKM)], Malaysia. He has more than 12 years of research and teaching experience. He has authored or coauthored numerous ISI and Scopus journals and IEEE conference papers. His research interests include interference management, millimeter-wave communication, ad-hoc networks, the Internet of Things, D2D communication, and quality of service enhancement for future wireless networks. He is also serving as a reviewer in more than 20 high reputation journals with different publishers, such as IEEE, Elsevier, Springer, Wiley, and Hindawi.